Levitated Dipole Experiment

J. Kesner
MIT Plasma Science and Fusion Center
Cambridge, MA 02139

M. Mauel
Department of Applied Physics, Columbia University
New York, NY 10027

Submitted to the U.S. Department of Energy
Notice DE-FG01-05ER05-09

Renewal of Grants DE-FG02-98ER54458/9

May , 2006

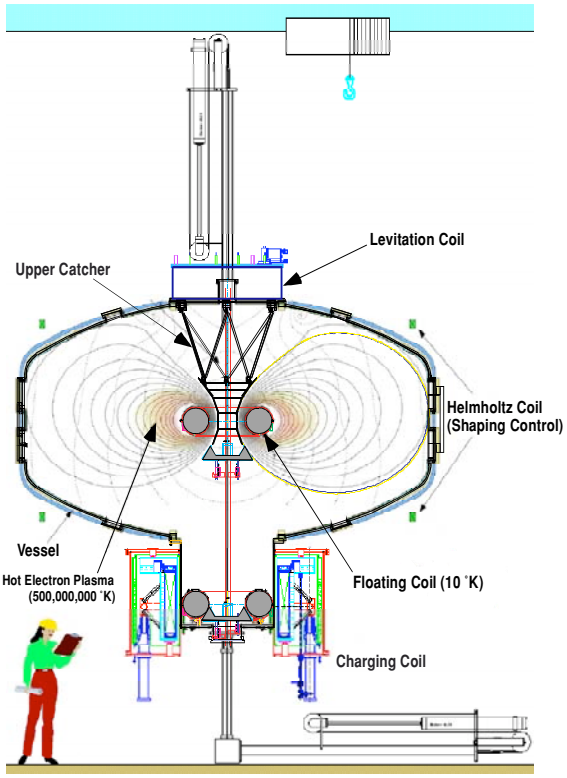

Contents

1 Executive Summary

The Plasma Physics Laboratory of Columbia University and the Plasma Science and Fusion Center (PSFC) of the Massachusetts Institute of Technology propose collaboratively to conduct experiments using the Levitated Dipole Experiment (LDX). These experiments are the next-step in our on-going research program to test the stability of high-beta plasmas in a dipole field, to measure and control particle circulation and adiabatic heating, and to measure and understand dipole plasma confinement at high beta.

The LDX experiment began operation in August 2004. Using multi-frequency electron cyclotron resonance heating (ECRH), high-beta plasmas have been created, sustained for many seconds, and studied while the high-field dipole magnet was mechanically-supported by three, thin (1 cm dia.) support rods. These experiments were the first stage of a carefully planned operational program that allows for the safe and reliable operation of the LDX superconducting magnets and the coordinated installation and test of diagnostics and research tools. During our first stage operation, significant programmatic and scientific results were achieved including: (i) demonstration of reliable operation of the high-field superconducting magnets, (ii) long-pulse, quasi-steady-state (> 10 s) plasma formation using ECRH, (iii) achievement of peak equatorial plasma beta near 20%, (iv) operation of all base diagnostics and data acquisition systems, (v) identification and parameterization of three discharge "regimes" having unique physics properties, (vi) preliminary study of ECRH profile control using multiple-frequency heating, (vii) identification of beta-limiting instability driven by a large fractional density of energetic trapped electrons, (viii) preliminary study of plasma shape effects, (ix) preliminary study of plasma density profile using movable edge probes and a single-cord microwave interferometer, and (x) preliminary study of x-ray emissivity using an array of x-ray detectors. These first-stage experiments, using a supported dipole, are now complete, and they have already met, or exceeded, all of our first-stage program objectives.

The present renewal proposal describes a three-year research program that carries out our next three operational stages. These next stages are: (i) levitated coil operation and investigation of dipole confinement and stability in high-temperature plasma, (ii) investigations of high-density plasma created with fast-gas injection, Li-pellet injection, and high-frequency (28 GHz) gryotron heating, and (iii) experiments with high-density plasma heating in order to investigate the energy confinement properties relevant to projected fusion power regimes. In order to carry-out these experiments, we will install several important new plasma control and diagnostic tools including: (i) our remaining three ECRH power sources having microwave heating frequencies at 10.5 GHz, 18 GHz, and 28 GHz, (ii) fast-gas nozzles for efficient and rapid fueling and impurity injection, (iii) edge bias probes to drive and control large-scale plasma convection for transport and adiabatic heating studies, (iv) a low-current (~ 14 kA·T) axial current-carrying conductor to investigate convective-cell and field-error control with weak toroidal field, (v) a low-cost Li-pellet injector to create and study the spatial homogenization of large density sources, (iv) two optical spectroscopy detector arrays to permit the measurement of impurity and plasma convection, and (v) a low-cost, pulsed plasma heating source (~ 100 kW) in order to investigate energy confinement and confinement scaling of plasma with density exceeding the cut-off frequencies of our microwave sources.

The overall objective of the proposed LDX research plan is to test whether fusion can benefit from nature's way to magnetically confine high-pressure plasma. The dipole fusion concept originated eighteen years ago [12] when it was learned that planetary magnetospheres have centrally-peaked plasma pressure profiles forming naturally when the solar wind drives plasma circulation and

heating. Unlike tokamaks, stellarators and RFPs, stable dipole confinement derives from plasma compressibility instead of the shear of magnetic field lines and average good curvature [49, 50, 51]. The dipole magnetic geometry can stabilize plasma at high volume-averaged beta, $\langle\beta\rangle \sim 1$, and peak beta, $\beta_{peak} \sim 10$ [2]. Additionally, the absence of magnetic shear is expected to decouple particle and energy confinement [22, 29, 24]. For these and other reasons, the dipole fusion concept offers an alternate path to fusion power. Conceptual design studies [32] show that dipole fusion power source requires the development of high field, high-temperature superconducting magnets but avoids both the use of tritium fuels and the need for expensive materials and breeding technologies.

A secondary, but also important, objective of the LDX research program is to create a innovative partnership between plasma scientists and magnet technology experts. By incorporating state-of-the-art engineering and design in its three superconducting magnets [3, 4, 5, 6, 7], LDX gains a unique and world-class research facility for long-pulse plasma physics research. The LDX superconducting magnets provide high magnetic confinement fields with over 1 MA·T in the Nb_3Sn floating coil for more than two hours of continuous experimentation. Additionally, the dipole geometry results in remarkable diagnostic access to very large volume plasmas enabling scientific experiments that have never before been possible.

The remainder of this proposal is organized into several parts and explicitly addresses each of the items requested in DOE Notice DE-FG01-05ER05-09. These are: (Sec. 3) a brief review of the physics basis for the dipole fusion concept, a short description of the LDX experimental device, and a description of the recent results from experiments conducted with a supported coil, and (Sec. 4) details of the proposed three-year research plan including our major research activities that will achieve our scientific objectives, and a summary of our research schedule, milestones, and deliverables. Because LDX is a unique facility and since it links fusion research to space plasma physics, the LDX project has attracted considerable public interest. Consequently, the LDX research plan incorporates educational and outreach activities. Attached separately from our Project Narrative, we have also prepared a short description of the LDX facility (that describes the superconducting magnets, plasma vacuum chamber, primary diagnostics, and support services) and a description of the LDX management plan as a joint research project of Columbia University and MIT's Plasma Science and Fusion Center. Finally, the LDX website, `http://www.psfc.mit.edu/ldx/`, describes the design and daily operation of LDX, lists 45 status reports describing the month-by-month fabrication of LDX, and presents several presentations, reprints, and preprints.

2 Abstract

LDX is a newly completed research facility with on-going experiments aimed to test whether fusion can benefit from nature's way to confine high-temperature plasma. The goal of the proposed renewal grant is to understand the equilibrium, stability and confinement properties for a plasma that is confined in the field of a levitated dipole. The proposed LDX experiments will yield new data on high-beta magnetic plasma confinement in a dipole magnetic field. They will be the first systematic investigations of the use of MHD compressibility to achieve stability with significant and highly-peaked plasma pressure. LDX will also provide the basis for understanding of (i) energetic particle confinement and stability in a dipole magnetic field, (ii) the relation between edge plasma and a hot plasma core, (iii) the possible elimination of drift-wave turbulence to produce plasmas with classical confinement, and (iv) the circulation and adiabatic heating of plasma confined by closed, shear-free magnetic field lines. Finally, LDX is an imaginative device that provides an excellent environment for training young scientists and stimulates interest in fusion research in the general public.

3 Background and Recent Accomplishments

This section presents a brief review of the physics basis for the dipole fusion concept, a short description of the LDX research facility, and a description of the recent results from experiments conducted with a supported coil.

3.1 Background

The dipole fusion concept was proposed in 1987 by Akira Hasegawa [12, 53, 54] who was motivated by observations of high beta plasma confined in planetary magnetospheres [57]. Unlike traditional toroidal configurations is which helical field lines define closed flux surfaces, the levitated dipole has closed field lines that define magnetic flux tubes having volumes that vary rapidly in radius. Hasegawa realized that the simple geometry of the dipole magnetic field results in a confinement concept with highly peaked pressure profiles that is nevertheless marginally stable to low-frequency magnetic and electrostatic fluctuations.

Since the time of Hasagawa's suggestion, and with the start of the fabrication of the LDX device, the theoretical basis for dipole physics has developed substantially by researchers at MIT, Columbia, UCLA, UCSD, U. Texas (Austin), and the Kurchatov Institute in Moscow. These recent theory efforts have lead to the evolution of the dipole concept while also supporting the scientific validity of Hasegawa's original concept. Advancements in dipole physics have been made in MHD stability, thermal and convective transport, and fusion power configurations.

Several authors have explored the ideal [2, 18, 19] and resistive MHD [25] properties of very high beta plasma equilibria, $\langle\beta\rangle \sim 1$, confined in a dipole field. The stability of drift frequency modes has been explored by Hasegawa and co-workers [13] and recently by Kesner, Simakov, Hastie and others [20, 26, 23, 27]. Convective cells and flows in closed field line configurations have been studied by a number of groups [21, 59] including PIC simulations by Dawson's group [29] and non-linear reduced MHD studies of Pastukhov and co-workers [22, 24, 30, 31]. The effects of non-axisymmetric magnetic field errors have been examined by Ryutov and co-authors [8] who estimated the magnitude of "neoclassical" electron thermal diffusivity.

Pastukhov and Sokolov [16, 17] have developed theories of thermal transport to the levitated ring when the surrounding plasma fully recycles neutrals and Mikhailovskii [28] has explored the effect of opening the field lines. Nonlinear gyrokinetic simulations have been developed to model experiments with the CTX device at Columbia University, and these simulations have successfully reproduced the global mode structures and nonlinear dynamics of both the collisionless interchange of energetic electrons confined by a dipole magnetic field [43, 44] and of the centrifugal instability excited by rapid plasma rotation [46, 47]. Krasheninnikova and Catto [48] have recently examined the fully electromagnetic stability of closed-field-line plasma containing energetic electrons.

Hasegawa and co-workers [13, 14] made initial explorations of dipole fusion power sources, and Teller, Fowler, and co-authors [15] have developed a conceptual design of a levitated dipole space propulsion system. More recently, Kesner and co-workers have explored a dipole fusion power source operating with ^{3}He catalyzed D-D fuel cycle that would eliminate both the difficulty of tritium breeding and the neutron damage and shielding requirements of the D-T fusion fuel cycle [32]. This design study showed the dipole fusion power source would have comparable mass power densities as possible advanced tokamak conceptual reactor [80] and significantly improved magnetic field utilization.

Recent theory has also guided our experimental program plan. The comparisons between measurements and developing theory is an essential element of the LDX program, and we expect continued theoretical studies will aid in planning and interpreting of upcoming LDX experiments.

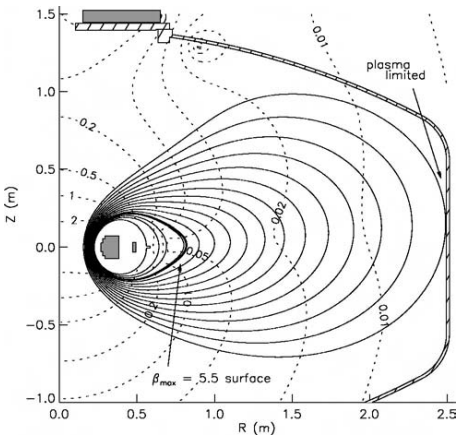

FIG. 2. High β equilibrium (β_{max}=10) solution in the LDX geometry.

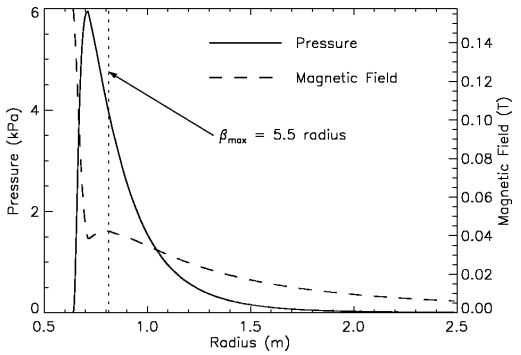

FIG. 3. Pressure profile and midplane magnetic field for an equilibrium with (β_{max}=10) solution in the LDX geometry.

Figure 1: Free-boundary calculations of high beta, $\langle\beta\rangle \sim 50\%$, diverted equilibrium for the LDX experiment (from Ref. [2]). This equilibrium was everywhere stable to MHD interchange and ballooning instabilities. (Left) Magnetic field lines and mod-B surfaces. The peak local beta is $\beta_{peak} \sim 10$. (Right) Equatorial profiles of the plasma pressure and magnetic field strength.

In order to provide further background, the following sections further introduce the physics of (i) MHD equilibrium and stability, (ii) drift and kinetic modes, (iii) energetic electron physics, and (iv) recent considerations for potential dipole fusion power sources.

3.1.1 MHD Equilibrium and Stability

For the dipole fusion concept, important topics in MHD equilibrium and stability include (i) equilibrium, (ii) high-beta stability through compressibility, (iii) resistive stability, (iv) convective cells, (v) magnetic shear and field errors.

MHD Equilibrium. The first step in the analysis of magnetic plasma confinement configurations is the investigation of ideal MHD equilibrium and stability. Garnier and co-authors [2] computed the first free-boundary equilibria for the levitated dipole configuration and developed target equilibria for the LDX experiment that were stable to all ideal MHD instabilities. The free-boundary equilibrium code, referred to as `DIPEQ`, can be run in either a predictive or interpretive mode to solve the Grad-Shafranov equation for arbitrary beta using reasonable models for the plasma pressure profile. These equilibrium calculations include the effects of external plasma shaping coils, central axial currents used to apply weak toroidal field, and internal poloidal plasma currents. The LDX shaping coils add an experimental capability to strongly modify the outer plasma shape, to change the flux expansion of the plasma, and to test the relationship between stability limits to the magnetic configuration. We have also computed equilibria with current flowing along an axial conductor and poloidal currents within the plasma. These add an experimental capability to add weak magnetic shear and limited ohmic heating. An example of very high beta equilibrium generated by the `DIPEQ` code is shown in Fig. 1. Analytical models for "point" dipole equilibria have also been derived [18], and these demonstrate the existence of MHD stable dipole equilibria at arbitrarily high local beta and support and illuminate the free-boundary computations.

High Beta Stability through Compressibility. According to ideal MHD theory, a plasma confined in regions of negative (or "bad") curvature will be marginally stable when the pressure profile, $p(\psi)$ satisfies the adiabaticity condition, $\delta(pV^\gamma) = 0$, with ψ the flux coordinate, γ the adiabatic constant, and $V = d(Volume)/d\psi = \oint d\ell/B$, the differential flux tube volume [49, 50]. For three-

dimensional adiabatic dynamics, $\gamma = 5/3$, and a necessary condition for MHD instability is $d_p \equiv -d(\ln p)/d(\ln V) > 5/3$. Notice this is a limit on the pressure gradient and not on the pressure. Thus a sufficiently large dipole plasma can have an arbitrarily large local beta value. As beta increases, the magnetic field is excluded from the region of the pressure peak on the outer dipole midplane.

Theoretical studies have shown that when a high-beta, dipole-confined plasma is stable to interchange modes it will also be stable to ideal ballooning modes [2]. The stability of ballooning modes at high beta has also been shown for a point dipole [19]. The adiabaticity condition leads to pressure profiles that scale radially as $p(\psi) \sim 1/V(\psi)^\gamma$. Gyrokinetic theory defines marginally stable density profiles that scale as $n(\psi) \sim 1/V(\psi)$. Thus, for adiabatic profiles, the value of $\eta \equiv d\ln T/d\ln n = \gamma - 1 = 2/3$. In a dipole magnetic field, $V(\psi) \sim r^4$, and the marginally stable pressure can increase rapidly with decreasing radius, $p(r) \sim r^{-20/3}$. Similarly, the adiabatic density profile scales as $n \sim r^{-4}$ and the temperature scales as $T \sim r^{-8/3}$.

The stabilizing effect of compressibility has been observed experimentally in the large mirror ratio LAMEX experiment [60], supporting the dipole concept. The earlier levitron or "spherator" experiments provided an illustrative contrast with a levitated dipole. In the levitron, the radial separation between the internal ring and the outer plasma boundary was determined by close-fitting limiters. When the toroidal field was strong, the flux tube volume was seen to scale with radius like a tokamak, $V \sim 1/q$, and stable plasmas could only be created when the applied vertical field was sufficiently strong to provide good average curvature. When the toroidal field was zero, the flux tube volume scaled approximately with radius as a hard-core z-pinch, $V \sim r^2$. Since the ratio of the plasma radius at the edge to the inner radius of the ring was typically less than two (about $1-1.5$), the ratio of the core pressure, p_0, to the edge pressure, p_{sol}, was limited by compressibility to $p_0/p_{sol} \leq (V_{sol}/V_0)^\gamma = (r_{sol}/r_0)^{10/3} \approx 1.5^{10/3} = 19$. In contrast, for the dipole, r_{sol}/r_0 can be made very large leading to $p_0/p_{sol} > 10^3$.

Resistive modes. Simakov and co-authors [25] have examined the resistive stability of the high beta point dipole and have shown that it remains stable to the relatively fast modes that grow at a rate proportional to a fractional power of the resistivity, $\gamma_\rho \propto \eta^{1/3}$. For high-beta dipole equilibria, only very slowly growing resistive modes are present that grow at a rate $\propto \eta$.

Stability of Convective Cells. Under many important circumstances such as strong local heating, the pressure profile can be driven to violate the MHD marginal stability condition. Recent simulations indicate that when this happens the plasma develops large scale convective cells which generate non-local energy transport of the required magnitude to prevent the pressure profile from significantly exceeding the critical gradient set by ideal MHD interchange [22, 24, 24, 31]. The nonlinear cascade of interchange modes into large spatial scales is expected [61] because interchange modes are two dimensional and enstrophy (in addition to energy) is conserved in two dimensions. The simulations show the MHD interchange criterion becomes a "stiff" limit on the pressure gradient in analogy with models of "profile consistency".

Convective cell formation has also been predicted by PIC simulations [29]. Such convective cells lead to rapid circulation of particles. Thus a dipole confined plasma may exhibit near classical confinement until the pressure profile obtains a critical gradient. Thereafter energy transport will prevent a further steepening of the pressure profile and it will be accompanied by rapid particle circulation. Convective particle circulation in plasmas with steep adiabatic profiles is advantageous to potential advanced-fuel fusion power sources [32].

Experiments in multipoles showed that convective cells can provide the dominant source of cross-field transport in shear-free systems. It is understood theoretically [63, 62] that zero frequency convective cells are closely related to interchange modes and they will grow in regions where $\delta(pV^\gamma) < 0$. In addition it has been shown that convective cells can exist in regions of "good

curvature" when the heating is non-uniform. In the Wisconsin octupole experiments the initial plasma was non-uniformly distributed and slowly-decaying convective cells were observed throughout the plasma [64]. These results suggest that the degree of heating and fueling uniformity will be important in a levitated dipole as a means to control the excitation of convective cells. These octupole experiments also indicated that a small amount of magnetic shear eliminates convective cell formation and that small field errors can cause convective flow patterns in an otherwise shear-free configuration [65].

Effect of Magnetic Shear and Field Errors. Ideal MHD theory predicts that the presence of magnetic shear will eliminate the compressibility term and give rise to Mercier modes at relatively low values of beta. However, Mikhailovskii and Skovoroda [28] have shown that when the adiabatic stability condition is maintained ($\delta(pV^\gamma) \geq 0$ i.e. $d_p \leq \gamma$) in the presence of weak shear, the destabilized Mercier modes give rise to weakly unstable sound waves. As a result the instabilities that would arise from the presence of weak shear have weak growth rates and that may be stabilized by non-ideal effects. In contrast, systems that do not satisfy the adiabatic stability condition, like tokamaks, excite fast Alfvén modes when the Mercier criterion is violated. Mikhailovskii and co-authors have called systems that satisfy the dipole's adiabatic stability condition, "well organized systems."

While sufficiently strong magnetic shear may create conditions for high-beta instabilities, magnetic shear has the beneficial effect of eliminating the wandering of field-lines due to field errors. Ryutov and co-authors [8] have computed the neoclassical electron thermal diffusivity that result from field errors in levitated dipole and FRC configurations. For conditions occurring in projected dipole fusion power conditions, the level of magnetic field errors must be very small, $\delta B/B_0 < 10^{-7}$, in order for the transport due to field errors to be less than classical collisional transport. Alternatively, by adding a weak toroidal field that is either larger than the field error or larger than the gryo-reduced field, $(\rho/L)B_0$, the effects of field-error transport are practically eliminated.

3.1.2 Drift and Kinetic Modes

Theoretical studies have been completed that examine (i) the drift stability of dipole confined plasma, and (ii) the particle losses associated with drift cyclotron modes.

Drift Stability in a Dipole Confined Plasma. Since plasma loss from a levitated dipole results from cross field transport, (and not from scatter into a loss cone as in planetary magnetospheres) we expect the distribution function will become isotropic. To lowest order the distribution function would be approximated by $F_0 = F_0(\epsilon, \psi)$ with $\epsilon = \mu B + v_\parallel^2/2$, the particle energy.

For a closed-field line system the MHD stability requirement is intrinsically related to the criteria for the stability of drift waves. Drift stability is characterized by two frequencies: the plasma diamagnetic drift frequency, $\hat{\omega}_{*n}$, proportional to the plasma density gradient, and the magnetic drift frequency, $\hat{\omega}_d$, proportional to the bounce-averaged magnetic curvature. One can define a frequency proportional to the plasma pressure gradient, $\hat{\omega}_{*p} = \hat{\omega}_{*n}/(1+\eta)$ (with $\eta = d\ln T/d\ln n$) and show that $d_p = \hat{\omega}_{*p}/\hat{\omega}_d$. The ideal MHD stability requirement, $d_p \leq \gamma$, is equivalent to the relation $\hat{\omega}_{*p}/\hat{\omega}_d = (\omega_{*i}/\hat{\omega}_d)(1+\eta) \leq \gamma$. Recalling that for a tokamak $\hat{\omega}_{*p}/\hat{\omega}_d \sim R/a \gg 1$, we observe that the MHD stability criterion for a dipole results in a very different ordering. In a dipole plasma, the diamagnetic drift is *comparable* to the curvature drift. The dipole's relatively weak pressure gradient has important consequences for drift waves.

Theoretical studies of drift frequency modes in a dipole [20, 26, 23] indicate that, in the region of negative curvature between the pressure peak and the wall, the stability is dependent on $\eta = d\ln T/d\ln n_e$. When $\eta < 2/3$ a drift-like instability known as the "entropy mode" can become unstable. Near the marginal stability boundary, $d_p \sim 5/3$, the MHD and the entropy modes will

couple. In the inner, "good-curvature" region, $\eta < 0$ is expected in large dipole confinement systems since the inward particle flux is fully recycled. In this regime, the entropy mode may also become unstable [23].

Drift Cyclotron Modes. Drift cyclotron modes are high frequency unstable modes ($\omega \sim \Omega_{ci}$) modes that are driven by temperature and density gradients. Pastukhov and Sokolov have evaluated the transport from these modes in the good curvature region near the surface of the levitated dipole [16, 17]. They show that the resulting transport would be severely limited by particle recycling at the surface of the internal coil. Because the surface of dipole is completely surrounded by a dense plasma, the net particle flux to the ring must vanish. A cool, high-density sheath is predicted to form at the dipole surface which transforms the thermal flux into bremsstrahlung radiation.

3.1.3 Energetic Electron Physics

Because fusion reactions produce energetic particles, the physics of energetic particles is an essential element of confinement physics. Since the discovery of geomagnetically trapped particles by Van Allen and co-workers [55], energetic particles are now known to play an important role in the dynamics of magnetospheres. Indeed, the radiation belts were used to develop and test concepts of adiabatic confinement and transport [56], and predicting variations in energetic particle flux is among the primary concerns of space weather prediction [58].

Energetic electron production has been used in many laboratory devices to produce high-beta plasma that contain trapped, relativistic or weakly relativistic electrons. The "Elmo" mirror and "Elmo bumpy torus" experiments [66] were among the earliest to demonstrate the efficient use of microwaves to create high-beta plasma containing trapped electrons. Energetic electrons were also created by microwaves in the FM-1b levitron [37]; stable hot electron plasmas were created in a minimum-B mirror device having $\langle\beta\rangle \sim 30\%$ [76]; and interchange instabilities excited by energetic electron plasmas confined by a mechanically-supported dipole have been extensively studied in the CTX device [38, 43, 44].

Since energetic particles have magnetic drifts that are comparable, or faster, than the MHD time scale for the lower-energy background plasma, the stability of plasmas containing energetic particles require a gyrokinetic treatment. Early theoretical studies of energetic electrons trapped in magnetic mirrors [67, 68, 69, 75] showed that potentially two unstable modes exist: (i) an MHD-like mode of the lower energy plasma modified by the charge uncovering of the decoupled hot electron population, and (ii) the hot electron interchange mode (HEI) which is a gyrokinetic instability of the hot electrons. The coupling between the lower temperature plasma and the energetic electrons was found to strongly influence stability. The diamagnetic well created by the hot electrons can stabilize the low-frequency MHD mode, provided that the pressure of the lower-temperature plasma is not too large [70]. The ion polarization currents of the background plasma can stabilize the high-frequency hot electron mode, even when the local pressure gradients of the hot electrons exceed the usual MHD instability threshold.

In LDX, electron cyclotron resonance heating (ECRH) creates a plasma with non-Maxwellian electrons having complex kinetic stability properties. Understanding the stability of plasma with non-Maxwellian energetic electrons remains a matter of study; however, we expect the stability of the cooler plasma to be limited by usual MHD considerations [48] while the pressure of the hot electron component is observed to be limited by the hot electron interchange (HEI) mode. As the density of LDX discharges increases, the pressure of the lower-energy (and denser) plasma also increases, which may reduce energetic particle effects.

The HEI mode is characterized by a real frequency proportional to the hot electron magnetic

drift frequency, ω_{dh}. For LDX, ω_{dh} is in the range of 0.5 to several MHz. The HEI mode propagates in the drift direction of the energetic electrons, creating drift resonances [38, 39] and complex nonlinear frequency sweeping [43, 44] that makes mode identification especially easy. HEI modes are global with low azimuthal mode numbers [43] that drive the distribution of energetic electrons to one that can be described by adiabatic invariants, $F_0(\mu,\ J)$, independent of magnetic flux, ψ, i.e. $\partial F_0/\partial\psi \sim 0$. For distributions of this type, the number of energetic electrons per flux tube is constant, satisfying the condition $\delta(n_h V) \sim 0$, or $d_{nh} \equiv -d\ln n_h/d\ln V = 1$. When the electrons are deeply trapped, $T_\perp \gg T_{||}$, then $\eta = 3/4$, and the stationary distribution satisfies $d_p = d_n(1+\eta) = 7/4$. A local gryokinetic dispersion relation for the HEI mode in a point dipole magnetic geometry has been derived [41] for the simplifying case when the electron distribution function, $F(\mu, J, \psi)$, can be separated into an adiabatic part and a part that varies only in ψ. In this case, the local stability condition for the HEI is $d_{nh} < 1 + (m_\perp^2/6)(\omega_{dh}/\omega_{ci})(n/n_h)$, a result that is similar to the one obtained by Krall [67]. Instability only occurs when the energetic electron density gradient exceeds a threshold exceeding the usual MHD stability limit for an isotropic and Maxwellian pressure profile. As the fraction of energetic electrons, n_h/n, increases, stability can still improve with increasing hot electron temperature, $\propto \omega_{dh}/\omega_{ci}$. Additionally, the HEI mode is global in extent [43], and electrostatic eigenvalue calculations show that the local instability criterion can be violated in thin regions while the HEI global mode remains stable.

3.1.4 The Dipole as an Advanced Fuel Energy Source

Studies by Hasegawa, *et al.* [13, 14] and by Teller, *et al.* [15] considered the application of a levitated dipole as a D-^{3}He based power source. Advanced fuel cycles (D-^{3}He, D-D) eliminate the need for tritium breeding and can significantly reduce 14 MeV neutron production and the associated structural damage. By incorporating an internal refrigerator in the floating ring a levitated dipole device would be intrinsically steady state. Such a device would deposit power on the first wall as surface heating, permitting a thin walled vacuum vessel and eliminating the need for a massive neutron shield. In a dipole the magnetic field is produced by a coil that is internal to the plasma and the plasma pressure falls off as the magnetic field falls off leading to a good utilization of the field. Therefore although the vacuum chamber envisioned is relatively large this does not lead to an unreasonably high magnetic field energy. Furthermore, there are no interlocking coil so that coil replacement could be relatively straight forward.

The D-D cycle is particularly interesting since the only fuel required is the plentiful deuterium. We have recently considered a dipole based system as a fusion power source [32] utilizing a fuel cycle which we call the "Helium catalyzed D-D" cycle in which the secondary ^{3}He is burned and the secondary tritium is recovered and reintroduced and burned later after decaying into ^{3}He. In this design study, representative power system configurations were presented, and three-dimensional neutronics calculations were performed in order to estimated the heating rates and temperatures that would occur within the floating coil. Although Nevins [78] found that a D-D cycle is precluded in a tokamak because of the accumulation of fusion products, in a dipole the combination of high beta and high energy confinement with reduced particle confinement would makes it ideally suited as a D-D based power source.

Besides parameterizing the overall dimensions and electromagnetic configuration of the D-D based fusion power source, it was also found to be relatively efficient. The ratio of plasma stored energy to magnet energy defined as $\beta_{global} = W_p/W_B$ is β_{global}= 0.096. For an tokamak reactor this ratio would be several times smaller. For example, the ARIES AT [80] advanced tokamak reactor study found W_B = 45 GJ, W_P=0.75 GJ, and β_{global}=0.017. The ratio $\beta_{global}(dipole)/\beta_{global}(aries) \sim 5.7$ indicates an improved utilization of magnetic field energy that

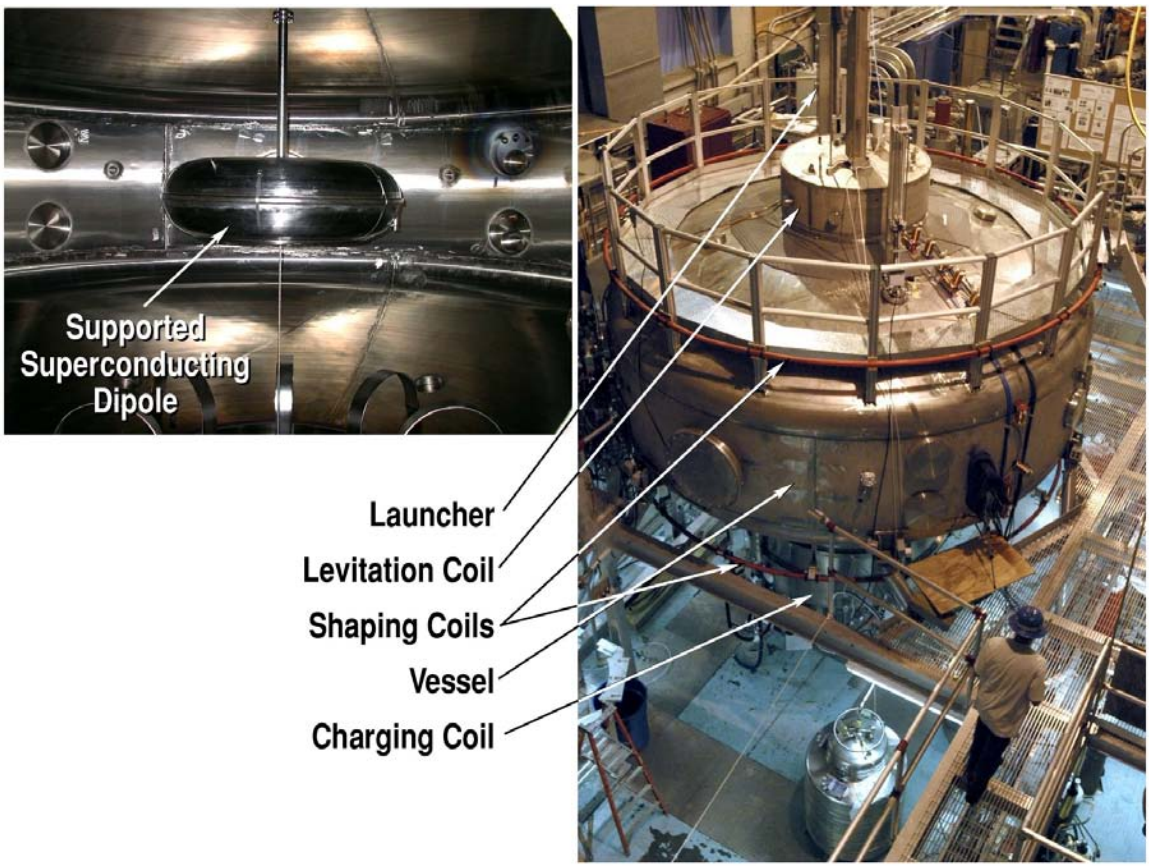

Figure 2: Photographs of the exterior (right) and interior (left) of the LDX experiment. The photographs show the configuration used for supported coil experiments and indicate the locations of the upper launcher, the levitation coil, the shaping coils, the vacuum vessel, and the charging coil.

results from the higher average beta that a dipole can support. In the "Helium catalyzed D-D" power cycle approximately 94% of the fusion power is produced as bremsstrahlung and particles leading to surface heating (with a relatively low wall loading). Nevertheless, although the ARIES AT wall loading (3.3 MW/m^2 from neutrons) exceeds the dipole reactor wall loading (photons and particles) by a factor of 40, the mass power density [79], *i.e.* the power per unit volume of structure (first wall and coil) for the dipole (1.1 to 1.75 MW/m^3) is comparable to the mass power density of ARIES, estimated to be 1.5 MW/m^3 (where the thermal power was 2 GW, and the system volume was 1300 m^3).

Although the D-T fuel cycle cannot be used in a dipole power source due to excessive neutron heating of the internal coil, seeding with tritium may be useful to ignite such a device. Furthermore the D-T cycle offers the possibility of a low-cost ignition experiment in which the internal coil is designed to have minimal shielding and to warm up inertially and float for an estimated 10 minutes after the start of plasma ignition [32].

3.2 Recent Accomplishments

The LDX experiment began operation in August 2004. This was a major milestone for the project and signified the completion of the fabrication three superconducting magnets, the installation of

phase-one plasma diagnostics, and the operation of our initial plasma heating and control systems.

During the past 1.5 years, experiments were conducted with the superconducting floating coil supported by three radial spokes. These experiments (i) demonstrated the safe and reliable operation of our superconducting coils, (ii) tested our base-case diagnostics and plasma heating tools, and (iii) initiated our exploration of the physics of high beta dipole confinement. Multi-frequency electron cyclotron resonance heating (ECRH) was used to create high-beta plasmas, and the microwaves sustained the plasma discharges for many seconds to allow detailed investigations with a variety of plasma diagnostics and cameras.

These experiments achieved, or exceeded, all of our first-stage program objectives. In particular, results obtained during initial experiments include: (i) demonstration of reliable operation of the high-field superconducting magnets, (ii) long-pulse, quasi-steady-state (> 10 s) plasma formation using ECRH, (iii) detection of peak equatorial plasma beta $\sim$20%, (iv) operation of all base diagnostics and data acquisition systems, (v) identification and parameterization of three discharge "regimes" having unique physics properties, (vi) observation of stability properties of the background, thermal plasma, (vii) preliminary study of ECRH profile control using multiple-frequency heating, (viii) identification of beta-limiting instability driven by a large fractional density of energetic trapped electrons, (ix) preliminary study of plasma shape effects, (x) preliminary study of plasma density profile using movable edge probes and a single-cord microwave interferometer, and (xi) preliminary study of x-ray emissivity using an array of x-ray detectors.

An essential addition to our experimental work has been the development of theoretical models that advance our understanding of the physics underlying the dipole fusion concept as explained in the previous section. These accomplishments include the identification of free-boundary LDX equilibria that are stable to ideal MHD modes with $\langle\beta\rangle \sim 1$ [2], the development of new gyrokinetic theory for drift stability [20, 26] and for convective cells [31], and the suggestion of a new fusion fuel cycle applicable to the dipole concept [32].

This section emphasizes the recent experimental accomplishments of the LDX Program. These are the completion of the fabrication of the LDX research facility and the start of LDX plasma physics experiments. Following a short description of the LDX facility, our key experimental results are summarized: (i) production of high-beta dipole confined plasma, (ii) observation of plasma instability in both the energetic and the thermal species, (iii) initial exploration of plasma pressure control using ECRH, and (iv) initial investigation of plasma shaping. These experiments have provided a basis for the understanding of our basic plasma control tools, multi-frequency ECRH, plasma shaping, and controlled gas fueling, that will be needed during our next research stages.

3.2.1 Building a New Research Facility

An important objective of the LDX research program is to create a innovative partnership between plasma scientists and magnet technology experts. By incorporating state-of-the-art engineering and design in its three superconducting magnets, LDX has gained a unique and world-class research facility for long-pulse plasma physics research. The LDX superconducting magnets provide high magnetic confinement fields with over 1 MA·T in the Nb_3Sn floating coil for more than two hours of continuous experimentation. LDX has also demonstrated the first use of a high-temperature superconducting (HTS) magnet during the full-current testing of the levitation coil. The dipole geometry gives the experiment a remarkably wide diagnostic access to large volume plasmas and enables scientific experiments that have never before been possible.

The LDX device is shown in Fig. 2. LDX consists of three circular and co-axial superconducting magnets [3], the floating coil [4, 5], the charging coil [4], and the levitation coil [7], a large cylindrical vacuum chamber, basic plasma diagnostics, two microwave ECRH heating systems, and two low

current shaping coils with independent power supplies.

The fabrication and assembly of the LDX experiment is a significant accomplishment that required an entirely new research facility to be built. During the previous grant period, the LDX research team has:

- Fabricated three superconducting magnets including the Nb_3Sn floating coil [4, 5] that operates in a persistent mode at high current and low weight and the levitation coil [7], fusion's first high-temperature superconducting magnet.
- Prepared the experimental hall including the construction of the vacuum vessel, discharge cleaning system, the experimental access platforms, the cryogenic systems, and the electrical power systems.
- Installed and operated the 2.45 GHz and 6.4 GHz microwave heating systems at full power and for long pulses.
- Installed and operated the coil handling systems including the pneumatic launcher that raises (lowers) the floating coil from (to) the lower charging station within the bore of the large superconducting charging coil.
- Installed the experimental control and data acquisition systems, including the plasma shaping coils and the digital gas puff controller.
- Designed, installed, and operated the basic diagnostic systems, including 26 channel magnetic detectors for equilibrium reconstruction, multiple visible cameras, multiple movable electrostatic probes, six x-ray detectors, high-speed digitizers for hot electron instability studies, internal Mirnov coils to measure high-beta magnetic fluctuations, single cord microwave interferometer, visible light photodetector array, and a single channel optical spectrometer.
- Developed our techniques of data analysis used to quantify and interpret our experimental measurements.

The design and entire construction of the LDX device has been recorded month-by-month and posted on our website's "Project News": `http://www.psfc.mit.edu/ldx/news.html`. The website has 40 reports and numerous photographs showing the superconducting magnets under all stages of construction, the vacuum chamber and site preparations, and the hard work and active oversight of the LDX research team. Technical descriptions of the LDX superconducting magnets and other experimental systems are also available in the "Facilities and Other Resources" section.

Since the start of LDX experimental operations in August, 2004, over 500 plasma discharges, each lasting between 4 and 12 seconds, have been studied in six campaigns. These experiments permitted us to develop (and practice) the cryogenic, magnetic, and mechanical procedures involved with cooling, charging, and launching the floating coil. All magnets have operated at full current. The total floating coil current ranged from 0.78 to 1.2 MA·T. This created fundamental electron cyclotron resonances that surrounded the floating coil for 2.45 GHz and 6.4 GHz microwaves.

3.2.2 Production of High-Beta Dipole Confined Plasma

The production of high-beta dipole confined plasma is a significant accomplishment. The LDX high-beta discharges represent the first time high-beta plasma has been created and sustained for long pulses in a laboratory dipole device. The production of high-beta plasma discharges required (i) the stabilization of the hot electron interchange (HEI) mode with the use of controlled gas

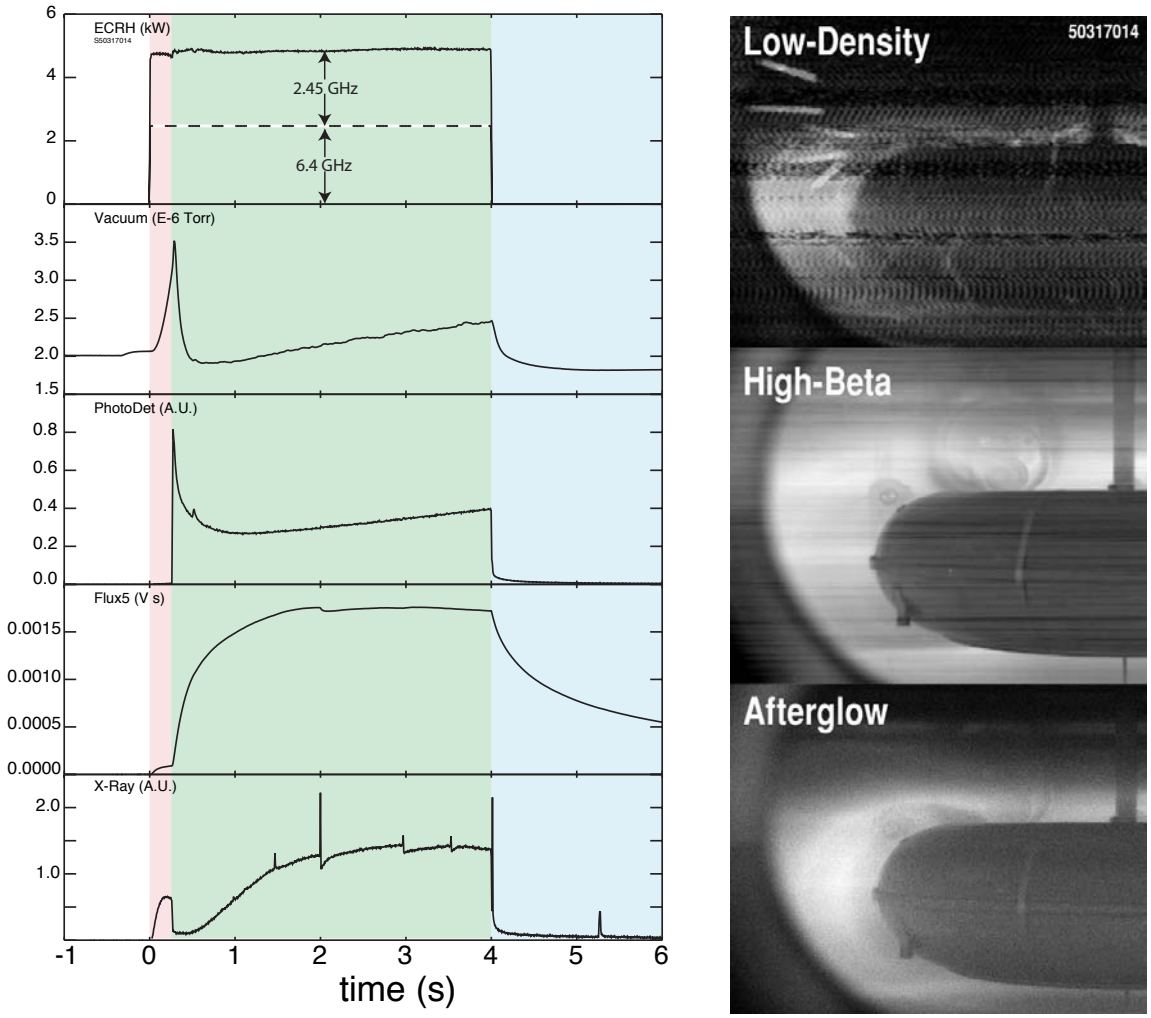

Figure 3: An example of a typical discharge (50317014) indicating three times characterized by low-density, high-beta, and the afterglow. (Left) Discharge time evolution indicating ECRH power (kW), vacuum ion gauge ($\times 10^{-6}$ Torr), light emission, plasma diamagnetism, and X-ray intensity (NaI detector). (Right) Visible light photographs taken during the discharge.

puffing to increase the plasma density, and (ii) the ability to continue to couple microwave power to hot electrons after the transition to higher plasma density has occurred.

High-beta dipole-confined plasma were produced using both single-frequency and multiple-frequency ECRH at power levels ranging from 2 kW to 5 kW. The microwave electron cyclotron resonances surrounded the floating coil, and the equatorial cyclotron resonance was positioned to create a population of magnetically-trapped, energetic electrons [38, 39]. X-ray emission was used to indicate the presence of energetic electrons, and the total plasma beta was detected using an array of magnetic field detectors and magnetic flux loops. Since the location of ECRH power deposition depends upon the resonance location, changes in the heating frequency and/or the floating coil current resulted in changes in the plasma pressure profile. However, our ability to create high-beta, hot electron plasmas was independent of the cyclotron resonance locations for the conditions

we have studied to date.

The rate of neutral deuterium gas fueling provides the essential experimental control that allows creation of high-beta plasma. This is illustrated in Fig. 3, which shows diagnostic signals from a typical LDX discharge. For this discharge, the floating coil was charged to approximately 0.9 MA·T, and the plasma was heated for 4 s with 5 kW of multiple-frequency ECRH at 2.45 and 6.4 GHz. In this discharge, three plasma regimes are observed: (i) an initial "low density" regime lasting 0.25 s, (ii) a "high-beta" regime that occurs after the neutral gas pressure has increased sufficiently, and (iii) an "afterglow" regime that occurs when the microwave power has been switched off and may last for many seconds as the energy stored in the magnetically-trapped hot electrons slowly decays. Each of these regimes have unique and interesting characteristics.

In the "low density" regime (during the first 0.25 s shown in Fig. 3), the plasma was characterized by a small rise in diamagnetism and low density as observed on a collimated photodiode. A significant x-ray signal is observed on a NaI detector, with a radial view that includes the floating-coil, which we believe indicates inward-moving hot electrons striking the surface of the coil. Negatively biased Langmuir probes at the outer edge of the plasma measure intense bursts of outward-directed energetic electrons. As will be explained, the low density regime undergoes a continuous bursting of the hot electron interchange (HEI) mode that resonantly transports energetic electrons radially [38, 39, 43]. Video images of "low density" discharges show the light emission is localized to the equatorial plane indicating the formation of a "disk" of deeply-trapped hot electrons. When the instability bursts becomes intense, the video images show inward transport of energetic plasma causing ablation and/or sputtering of dust and material from the outer, low-field side of floating coil.

The transition to the "high beta" regime is observed to occur when the neutral gas pressure exceeds a critical level (shown in Fig. 3 at 3.5×10^{-6} torr at $t = 0.25$ s for shot 50717014.) The level of neutral gas fueling required for the transition depends upon the conditions of the vacuum vessel, the ECRH heating power, and the outer shape of the plasma. The transition typically occurs within 2 ms and coincides with a buildup of plasma density. The buildup plasma diamagnetism occurs over a much longer 0.5 s interval. Initially, as the density rises, the detected x-ray intensity decreases by an order of magnitude consistent with the elimination of inward hot electron flux to the floating coil. The negative bursting stops, and the negatively-biased edge probes collect ion saturation current. Low frequency magnetic and electrostatic fluctuations appear that have characteristics that are very different from the HEI mode. If the rate of neutral fueling decreases sufficiently, a rapid and very intense burst of the HEI mode will occur causing a loss of stored energy and a return to the "low-density" regime. Video images of "high beta" plasmas show the light primarily emitted from a bright "halo" surrounding the floating coil. Abel inversion of the light emission shows the light to be significantly reduced within the "halo" indicating that the primary source of neutral fueling is from large radii and that the plasma is sufficiently hot and dense to limit the neutral penetration near the core. The video images also show "high-beta" plasmas do not cause ablation of dust from the floating coil, but instead shows a bright warming of the three floating coil support rods indicating the power deposition to the support rods significantly increases during the high-beta regime.

When the microwave power is switched off, the plasma enters the "afterglow" regime (shown in Fig. 3 to occur for $t > 4$ s). The behavior of the afterglow plasma also depends upon the rate of neutral fueling. If the neutral pressure is sufficiently high, the energetic trapped electron population slowly decays with a characteristic time scale of the order of 1 s. On this time scale, video images of the afterglow show the light emission to be peaked on the equatorial plane. As the neutral fueling is decreased, bursts of HEI instability appear that may cause either minor or major loss of stored energy.

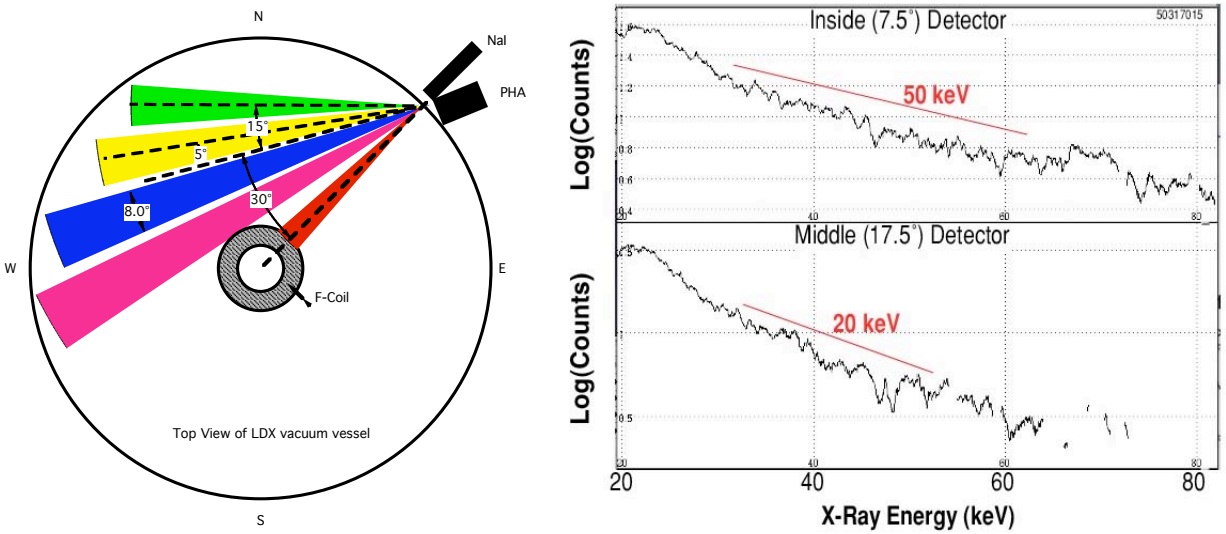

Figure 4: (Right) Pulse-height analysis of the time-integrated x-ray spectra measured with collimated CZT detectors. For this discharge (50513015), only 2.45 GHz heating was applied. Under these conditions, the intensity of target x-rays produced from the impact of electrons with the floating coil was substantially eliminated and allowed for a more accurate measurement of the electron bremsstrahlung spectra. The two collimated detectors show a centrally-peaked hot electron temperature and density.

ECRH creates non-Maxwellian electron populations [73] and trapped energetic electrons. Pulse-height analysis of the electron's bremsstrahlung radiation provides an indication of the energetic electron energy. Because the HEI mode transports electrons radially, electron-target x-rays created by the impact of electrons with the floating coil are also detected. However, we have observed a significant decrease of target x-ray production when only 2.45 GHz ECRH is applied and when the plasma enters the stable "high beta" regime. The intensity of x-rays measured by a NaI detector that is collimated to view the floating coil decreases by nearly two orders of magnitude under these conditions. Fig. 4 shows the measured x-ray spectra for high-beta plasmas during 2.45 GHz only heating. The diagnostic uses cadmium-zinc-telluride (CZT) detectors with an energy range of 10 to 740 keV. The integrated spectra shows a non-Maxwellian distribution that is characterized by effective "temperatures" in the range of 20-50 keV. Four CZT detectors were used to view the plasma as a function of radius, and these indicated that the energetic electrons density and temperature were centrally-peaked near the floating coil.

Magnetic measurements provide a diagnostic for determining the plasma diamagnetic ring current, the current centroid location (or magnetic dipole moment), and the induced changes in the floating coil current due to its superconducting flux constraint. The magnetic flux is measured by eight loops encircling the vacuum chamber at various locations, and the magnetic field, both normal and tangential to the chamber wall, is measured at eighteen locations with Hall probes and pick-up coils. Because the magnetic flux from plasma current links the superconducting floating coil, as the plasma current increases, the total current in the floating coil decreases. Since the magnetic measurements detect changes in both the plasma current and the floating coil current, we use a constrained least-squares method to estimate the plasma current and plasma dipole moment. Fig. **??** shows the evolution of the currents and of the plasma current centroid that best fit the diamagnetic measurements. The location of the current centroid indicates the position of the peak

gradient of the pressure, and the centroid is observed to move substantially during a discharge.

Reconstructions of the plasma's anisotropic pressure are made by computing the least-squares best-fit of a model to the magnetic diagnostics. We use an anisotropic pressure profile, with $P_\perp > P_{||}$, given by $P_\perp(\psi, B) = \hat{P}(\psi)(B_0(\psi)/B)^{2p}$ [83], where $\mathbf{B} = \nabla\phi \times \nabla\psi/2\pi$ and $B_0(\psi)$ is the minimum field strength on a field-line. With this model, the ratio of perpendicular to parallel pressure is constant over the plasma, $P_\perp/P_{||} = 1 + 2p$. To fit this model to the magnetic measurements, the plasma current, $J_\phi(r, z)$, is related to the pressure through the self-consistent equilibrium, $\psi(r, z)$. However, since the dipole moment of J_ϕ is less than 2% of the coil's magnetic moment, the difference between the vacuum dipole field and the self-consistent field is undetectable for the beta achieved to date. Using the dipole's vacuum field, the plasma ring current density can be computed from any given function of $\hat{P}$ and parameter p using

$$J_\phi = -2\pi r \left[D_\psi P_\perp + 2p P_\perp D_\psi \ln B/(1+2p) \right] , \quad (1)$$

where $D_\psi \equiv |\nabla\psi|^{-2}\nabla\psi \cdot \nabla$. The detected signal from a magnetic sensor is computed by combining contributions from J_ϕ throughout the plasma with the decrease of I_d required to maintain constant the flux linked by the superconducting dipole. For the reconstructions reported here, $\hat{P} = \Delta(\psi) \times P_0(\psi/\psi_0)^{4g}$, where $\Delta(\psi) = [(\psi - \psi_d)/(\psi_0 - \psi_d)]^\alpha$ is chosen to vanish at the surface of the dipole, ψ_d, and to equal unity at the location of the pressure peak, ψ_0. Far from the coil's surface, where $|\psi| \ll |\psi_d|$, the equatorial pressure is $P_\perp(r) \approx P_0(R_{peak}/r)^{4g}$. This form resembles the MHD condition for marginal stability, expressed as $\delta(PV^\gamma) = 0$ with $\gamma = 5/3$, that is equal to $P \sim r^{-4\gamma}$ in a dipole [2, 84, 49, 51].

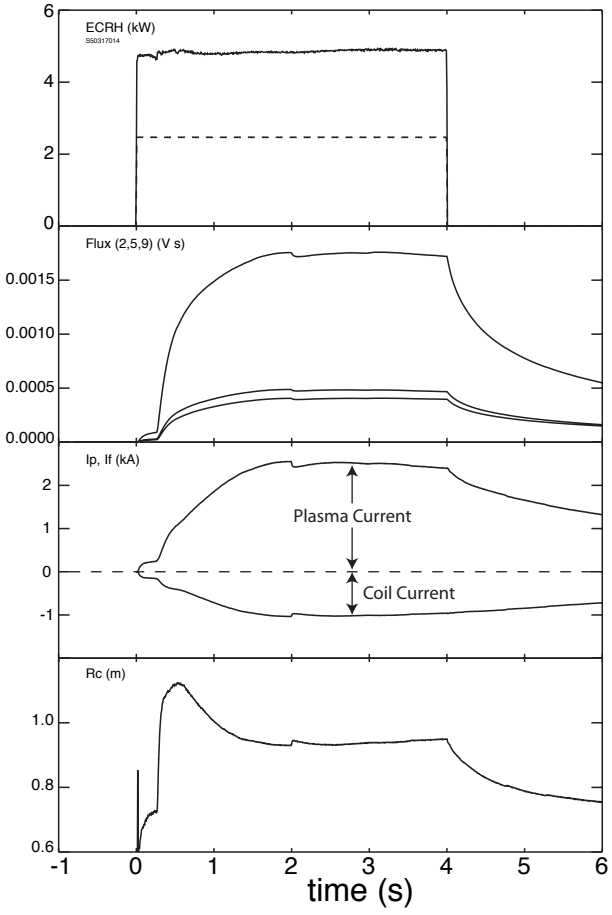

Figure 5: Discharge 50317014 showing RF power, diamagnetic flux loop measurements, plasma and floating coil current evolution, and location of the plasma current centroid.

The four free parameters of the model are p, ψ_0, g, and P_0, corresponding to anisotropy, pressure peak location, profile width, and total plasma current, respectively. These are the parameters that are varied to find the best-fit to the magnetic and x-ray data. With four unknown parameters and 26 magnetic measurements, a value of $\chi^2 \approx 22$ corresponds to a 50% confidence in the goodness of fit.

As is necessary when reconstructing the magnetospheric ring current of the (effectively flux-conserving) Earth using ground-based magnetometers [52], equilibrium reconstruction in LDX also requires that the magnetic flux linking the superconducting dipole coil be maintained constant. The dipole current decreases as the plasma diamagnetic current increases. The current decrease ΔI_d is proportional to the mutual inductance between the plasma and the dipole coil, which is a property of the equilibrium pressure profile. Typically, $\Delta I_d \sim -I_p/5$.

The fact that the floating coil current decreases in the presence of plasma limits the ability of the magnetic diagnostics, located on the vacuum vessel, to resolve different pressure and current profiles having the same dipole moment. The present magnetic diagnostics are most sensitive to lowest-order magnetic dipole moments. Because the magnetic sensors pick up the sum of ΔI_d and I_p and since they have opposite signs, the change in dipole current, ΔI_d, contributes significantly to the total quadrupole moment. Higher order moments of the plasma current will be measured in future experiments using flux loops installed near the axis.

Fig. 6 shows the results of magnetic equilibrium reconstruction constrained by 2D x-ray images. Two different discharges are shown. The top figure shows the x-ray image and reconstructed equilibrium pressure contours when 2.5 kW of only 2.45 GHz was applied. The bottom figure shows the results with the application of 2.5 kW of only 6.4 GHz heating. The images from the x-ray camera showing the line integrated emissivity are also superimposed on the visible light pictures. In each case, x-ray emissivity data is used to constrain the peak pressure location, and it indicates a high degree of pressure anisotropy. Since the pressure results almost entirely from energetic trapped electrons, the x-ray image is expected to be well correlated with the peak pressure profile. Abel inversion of the x-ray images as well as the light emission during the afterglow period (after the microwave power has been switched off) are consistent with the pressure peak located at the fundamental cyclotron resonance of the injected microwaves. The effect of anisotropic pressure is also evident in these contour pictures. The pressure contours do not coincide with flux contours, and the pressure becomes more localized to the midplane as it becomes more anisotropic.

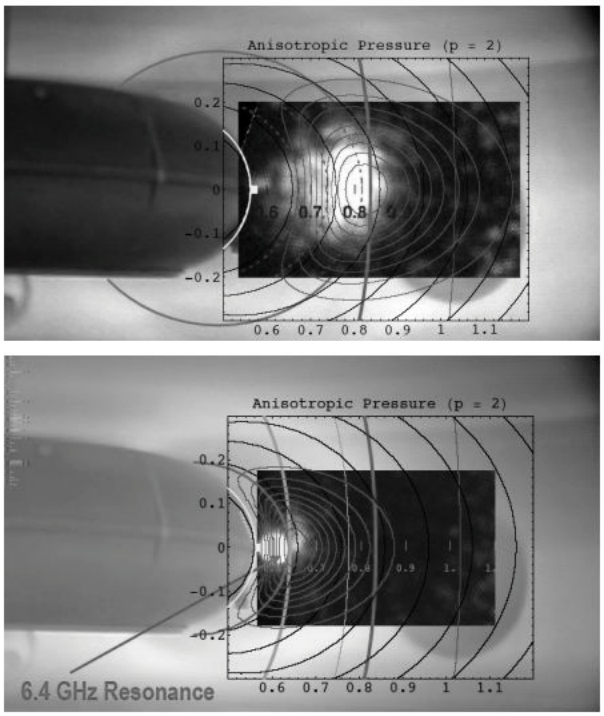

Figure 6: Contours of the reconstructed pressure profiles superimposed onto the x-ray images measured during (top) 2.45 GHz heating and (bottom) 6.4 GHz heating.

Plasmas with the highest values of I_p and β are created by combining both 2.45 and 6.4 GHz heating frequencies. However, the x-ray images do not show a clear pressure peak, and we suspect that the pressure profile may not be as well represented by the model profile defined above. The sum of the mean-square deviations between the best-fit model profile and the magnetic measurements doubles as compared with single-frequency heating, and this may be related to the presence of two pressure peaks, one at each resonance. If R_{peak} is assumed to be midway between the resonances and $p = 2$, then 5 kW of heating creates a best-fit plasma (Shot 50513029) with $I_p = 3.5$ kA, $\Delta I_d = -0.8$ kA, $W_p = 330$ J, $g = 2.8$, peak perpendicular pressure of 750 Pa, and maximum local beta of $\beta = (2\beta_\perp + \beta_{||})/3 = 21\%$. If R_{peak} moves outward and closer to the 2.45 GHz resonance by 5 cm, the best-fit gives $\beta = 23\%$; moving it inward by 4 cm towards the 6.4 GHz resonance results in the best-fit of $\beta = 18\%$. Fig. **??** shows the contours of the pressure and current profiles for the best-fit, highest $\langle\beta\rangle$ discharge.

Since the magnetic sensors are primarily sensitive to the plasma dipole moment, the x-ray emis-

sivity image is used to constrain the location of the pressure peak. The x-ray images show that the peak pressure occurs at the fundamental resonance of the heating frequency during singe-frequency heating and in between the two resonances during two-frequency heating. The reconstructed pressure profiles have a slightly steeper profile than allowed by the ideal MHD stability condition, and the peak local beta exceeds 20%. In future experiments with a magnetically levitated dipole, the magnetic diagnostics will be improved by adding new flux loops near the axis and strongly coupled to the induced changes in the dipole current. The resulting improvement in the magnetic reconstruction is illustrated in Fig. **??**. This figure compares contours of χ^2 at the 50% and 25% confidence levels as a function of two profile parameters, g and R_{peak}. With the existing magnetic sensors, a family of profile parameters fit the magnetic data equally well since these profiles have equivalent plasma dipole moments. When three new flux loops are installed on axis, magnetic reconstruction is able to constrain the radial location of the pressure peak and the profile steepness without requiring independent x-ray observations.

Estimates of the energetic electron parameters can be made from the reconstructed peak pressure and the detected x-ray spectra Fig. 4. Assuming that $T_{eh} \sim 50\ keV$ as measured by the x-ray pulse height analysis, the equilibrium reconstruction implies a hot electron density $n_{eh} \sim 3 \times 10^{16}$ m^{-3} at the peak pressure location ($P_0 \sim 220$ Pa). Since the magnetic field decreases with radius more quickly than the radius near the pressure peak, the peak plasma beta occurs at 0.95 m. With $\beta_{max} \sim 20\%$ and T_{eh} the same as before, implies a hot electron density of $n_{eh} \sim 10^{16}$ m^{-3}.

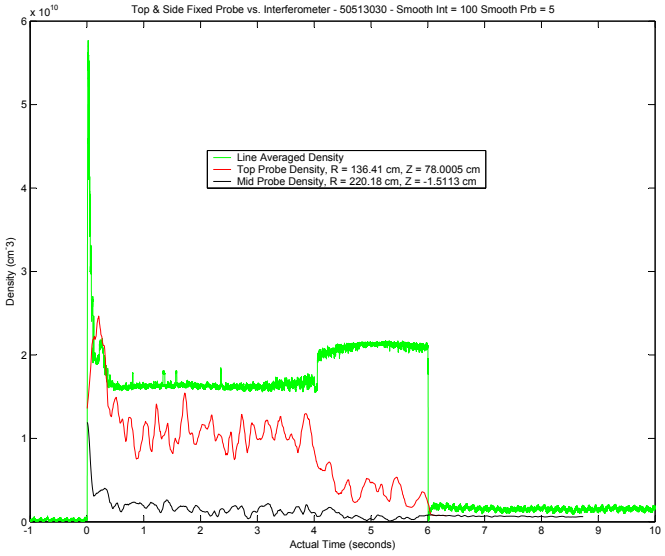

Figure 9: Discharge 50513030 showing line average and edge probe density. The rate of neutral gas fueling was decreased at $t = 4$ s, and the rapid disappearance of the density at $t = 6$ s corresponds to the end of the ECRH heating pulse and the occurrence of an intense HEI burst.

Two Langmuir probes, which enter the plasma on the outer midplane and from an upper port, were utilized to measure edge temperatures and densities. The edge density, n_{sol} is typically $n_{sol} \sim 2{\times}10^{16}$ m^{-3} and electron temperature is $T_{sol} \sim 10$ eV indicating a pressure $P_{sol} \sim 0.03$ Pa. The density along a midplane cord was measured using a 60 GHz microwave interferometer. These measurements give a line-averaged density of 2-3$\times10^{16}$ m^{-3}. If we assume the central density scales with radius such that $\delta(nV) \sim 0$ (so that $n \sim 1/r^4$), then the peak core density is $n_0 \sim 2{\times}10^{17}$ m^{-3}. (This density is about three times higher than the cutoff density for 2.45 GHz and one-half the cutoff density for 6.4 GHz heating.) If the density is much less peaked, scaling instead with radius as $n \sim 1/r$, then the peak density would be five times smaller, $n_0 \approx 4 \times 10^{16} \sim 2 \times n_{sol}$ m^{-3}. Fig. 9 compares the core line-average density with the edge probe measurement for a 6 s discharge with 5 kW microwave heating. Notice that after the rate of neutral gas fueling decreases at $t = 4$ s, the core density rises and the edge density falls. Later, at $t = 6$ s when the ECRH was switched off, the neutral fueling was insufficient to maintain stability during the afterglow, and the HEI mode caused a rapid decrease in density along with a nearly complete loss of plasma stored energy.

We conclude that LDX has succeeded in entering a stable high beta operating mode. The transition from the low-density regime to high-beta is only possible with sufficient gas fueling. This

requirement is consistent with the need to stabilize the HEI mode with a sufficient density of non-energetic "warm" or "cold" plasma density. If the neutral fueling rate is maintained, the high-beta plasma can be maintained in quasi-steady conditions for long pulse lengths.

3.3 Collective Plasma Modes in an ECRF Heated Plasma

In a dipole field the plasma between the internal coil and the pressure peak is confined in "good" curvature while the plasma between the pressure peak and the outer wall-limiter or separatrix is in "bad" curvature. Consideration of the MHD stability of the background plasma in the bad curvature region leads to the MHD requirement:

$$d_P = -\frac{d\ln p_b}{dlnV} \leq \gamma \tag{2}$$

with V the differential flux tube volume, $V = \oint d\ell/B$. In LDX, the MHD modes should be in the $f \sim c_s/L \sim 50$ KHz frequency range. The presence of a hot electron species leads to a some modification of Eq. (2) [**?**].

Non-linear studies indicate that in the presence of strong MHD driven flux tube mixing the density will obtain a profile:

$$d_n = -\frac{d\ln n_b}{dlnV} \sim 1 \tag{3}$$

When both of these equalities are satisfied $\eta \equiv d\ln T/d\ln V = 2/3$. The peaking of density implied by $d_n \sim 1$ may however be prevented by the ECRF accessibility requirements which limit the density for which the heating waves can penetrate the plasma. The stability of low frequency modes depends on the characteristic frequencies $\omega_\star = (k_\perp\rho)v_{th}\nabla n_e/n_e$ the diamagnetic drift frquency and $\omega_d = (k_\perp\rho)v_{th}\nabla V/V$ the magnetic drift frequency. In a traditional confinement device like a tokamak $\omega_\star \gg \omega_d$ whereas in a dipole confined plasma the stability criteria in Eqs. (2) and (3) will determine that $\omega_\star \sim \omega_d$.

The linear properties of drift frequency modes in a closed line system such as a dipole have been examined [**?**, **?**, **?**]. In the collisional regime a mode termed the "entropy mode" is predicted to appear beyond the pressure peak when $\eta < 2/3$ with a frequency $\omega \sim \omega_{di}$. The entropy mode tends to be flutelike along the field with $k_\perp\rho \leq 1$. It remains electrostatic and the dispersion relation is only slightly modified by finite beta[**?**] or collisionality [**?**] effects. For $T_e = T_i$, $Re(\omega) \sim 0$, but for $T_e > T_i$ (as in ECRF heated plasmas) $Re(\omega/\omega_{di}) > 0$. Assuming $T_e \sim 100$ eV and $k_\perp\rho \sim 0.1$ in LDX, this mode should be potentially unstable in the $1 < f < 5$ KHz range. The entropy mode is linearly unstable in the bad curvature region when $\eta < 2/3$ and in the good curvature region when $\eta < 0$.

Because the accessibility condition can be inconsistent with Eq. (3) there may be a tendency of dipole confined plasmas to become over dense. If this were to occur ECRF waves would be reflected before reaching the resonance heating region and the buildup of plasma density and pressure will cease. The plasma density would then be expected to fall to a sub-critical level within a confinement time and the buildup process will restart. For a 10 ms confinement time the frequency associated with this process would be ~ 100 Hz.

High Frequency instability due to Hot Electrons

Two types of high frequency plasma fluctuations are observed that indicate a plasma instability processes: (i) hot electron interchange (HEI) fluctuations near the magnetic drift frequency of the energetic electrons, ~ 1 MHz, and (ii) microwave bursts > 1 GHz that appear when the HEI mode

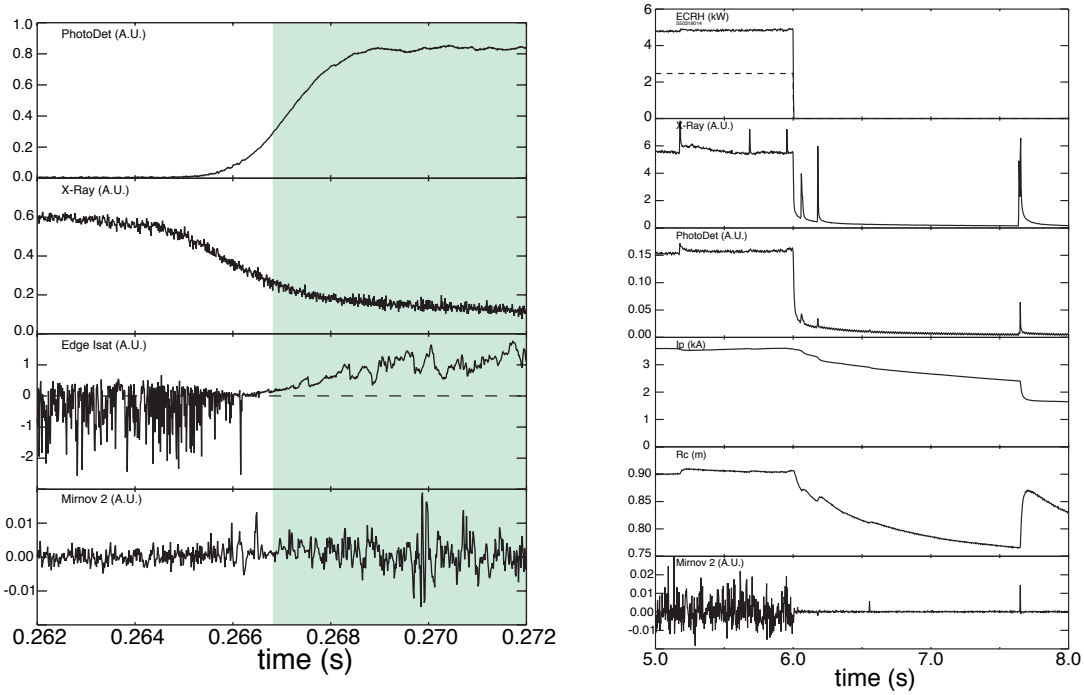

Figure 10: Expanded time intervals of discharge 50317014 showing (left) the transition from the low-density regime to the high-beta regime, and (right) the time near the end of the ECRH pulse when small HEI relaxation events occur during heating and events with larger loss in plasma stored energy occur during the afterglow.

causes rapid energetic electron transport. We are able to identify the gyrokinetic HEI mode because it has unique spectral characteristics when excited in the dipole magnetic field [38, 43]. We believe the high-frequency cyclotron mode may be a whistler [77] or an electron cyclotron maser instability excited by inverted velocity-space distributions created by drift-resonant radial electron transport caused by the HEI mode. At the present time, we have not measured the global mode structures nor the precise conditions for the appearances of these instabilities.

The dominate plasma instability in our first stage experiments is the HEI mode. This instability has a frequency near the magnetic drift frequency of the energetic electrons making it relatively easy to identify. The instability appears as bursts that rapidly repeat during the low-density regime and that also appear occasionally in high-beta plasmas during the high-beta and afterglow regimes. The HEI mode causes rapid radial transport of the energetic electrons as evident from outward-directed energetic electron current detected by edge probes, target x-rays created from inward-directed electrons, and rapid changes in the plasma stored energy and plasma current centroid detected by diamagnetic flux loops. Since observations of the HEI mode include instabilities occurring at high beta, LDX has been able to make the first measurements of the electromagnetic fluctuations of a high-beta gyrokinetic interchange mode.

Fig. 10 illustrates measurements of plasma instability in the LDX device at two times during a typical discharge. The left-hand figure shows a 10 ms interval at the transition from the low-density regime to the high-beta regime. Before the transition, $t < 0.267$ s, the the negatively-biased Langmuir probe detects bursts of electron current. After the transition, low-frequency fluctuations are observed in both the ion saturation current and the Mirnov detector. The right-hand figure shows the end of the ECRH heating pulse and the afterglow regime. During microwave heating,

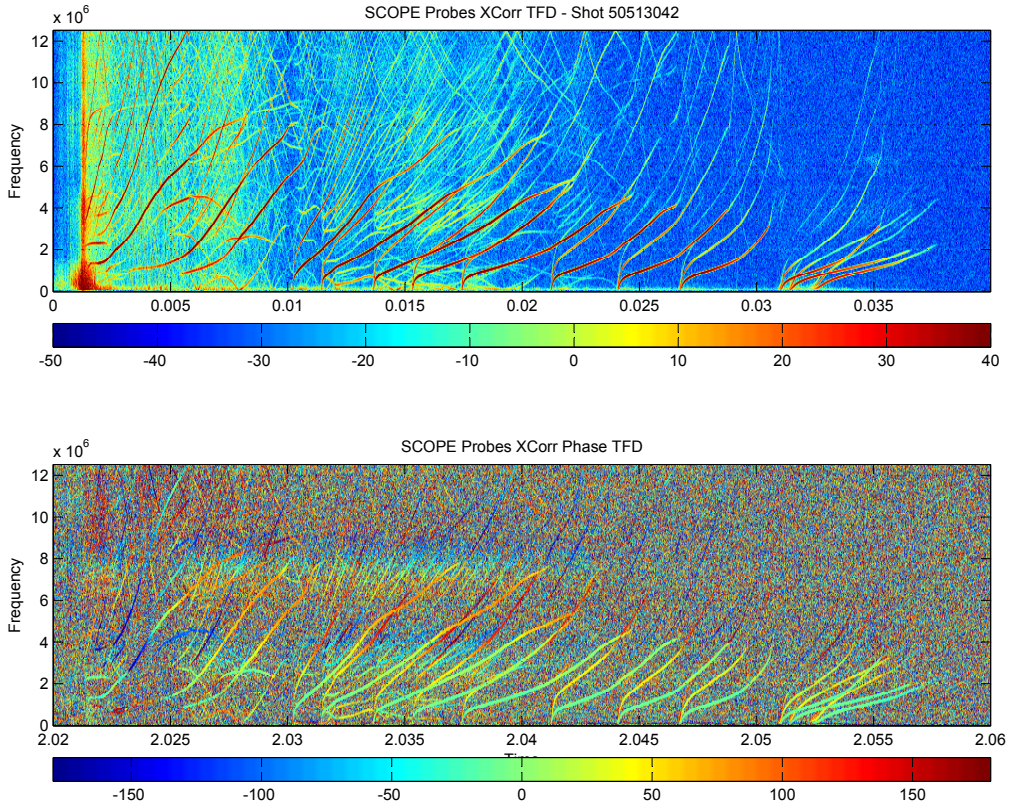

Figure 11: The amplitude (top) and phase (bottom) of the correlation between the signals detected with two high-impedance floating-potential probes. Many low-order modes are excited simultaneously and drift-resonate with trapped energetic electrons. The frequency spectrum clearly identifies the instability as a HEI mode.

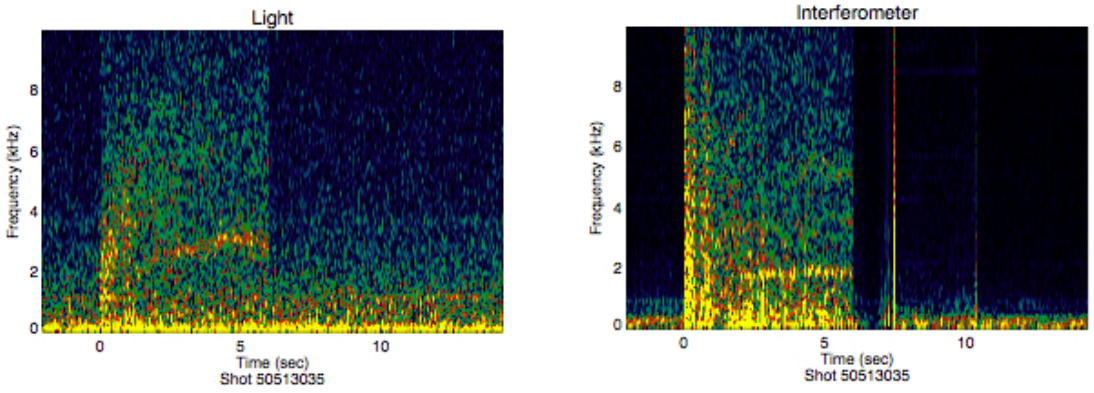

Figure 12: The time-frequency spectrograms of the low-frequency fluctuations of the visible light emission and the line-integrated plasma density. For this discharge, 50513035, a discrete mode with a frequency near 2 kHz is observed.

occasional bursts of the HEI mode cause fast relaxation events that cause an outward expansion of the plasma ring current and also an inward flux of energetic electrons. During the afterglow, similar relaxation events occur. When the level of neutral gas fueling is low, these events can cause significant fractions of the plasma stored energy to be lost.

The HEI mode is identified by it's spectral characteristics. The signals from high-impedance floating-potential probes were recorded by high-speed digitizers that were triggered by the bright x-ray or light bursts caused by rapid hot electron transport. Fig. 11 shows the time-frequency spectrogram of the amplitude and phase of two high-impedance probes separated toroidally by 45 deg. Several low-order azimuthal modes are excited simultaneously with frequencies that correspond to the drift-resonances with a wide range of hot electron energies. As the mode saturates, strong frequency sweeping occurs that indicates collisionless wave-particle interactions with weak non-resonant dissipation [44].

The low frequency mode often appears during the heating phase as a discrete mode of ∼1 kHz along with several harmonics. The mode amplitude increases with increasing heating power. The low-frequency mode is observed on several diagnostics, notably edge Langmuir probes and Mirnov coils as well as the photodiode and interferometer. It may be more pronounced on one or another diagnostic which may indicate that more than one mode may be present. Fig. 12 shows measurements of the low-frequency fluctuations observed during the high-beta regime with a visible light detector and with the microwave interferometer. The characteristics and causes for the fluctuations are presently not known.

Low Frequency instability due to Background Plasma

In LDX Langmuir probes measure an edge electron temperature of $T_{eb} \sim 10$ eV implying a core temperature of several times this value. The background electron species account for most of the density $n_{eh}/n_{eb} < 0.1$ whereas the hot species dominates the plasma stored energy.

Consider two discharges from the 5/13/05 experimental campaign in a well conditioned machine. Various diagnostic measurements shown in Fig. **??**. About 5 kW of ECRF power was applied to the plasma, equally divided between 2.45 and 6.4 GHz which are resonant on the outer midplane respectively at 5 cm and 20 cm from the floating coil. In discharge #31 the gas puffing system was disabled at t=4 s at which time the base pressure was measured to be 4.4×10^{-7} torr. In discharge #37 the base pressure was 3.9×10^{-7} torr before a gas puff at t=3 s. Figure **??** shows the time-frequency plot for these shots. Notice the initial frequency is 3.5 KHz in #31 and 3.8 KHz in #37. These frequencies fall into the range expected for an entropy mode. Noting that $\omega_{di} \propto \sqrt{T_i}$ the higher frequency observed in the latter shot may indicate an increased ion temperature associated with a reduced base pressure.

The gas feed experiments are consistent with T_i rising with a falling base pressure. The gas feed was turned off at t=4s in shot #31, and the mode frequency initially rises and later appears to loose coherence as a single well defined mode. In the gas puff experiment, shot #37, the mode frequency initially falls and later reappears as a lower frequency and broader spectrum of modes. It is also seen that the gas puff is accompanied by a rapid (3 fold) rise in both core and edge density (measured with both an interferometer and edge Langmuir probes), which will tend to reduce η and $\omega_\star$ which are parameters in the linear dispersion relation. (The plasma diamagnetism falls more slowly, presumably related to a loss of hot electrons due to pitch angle scatter on the neutral gas). Fig. **??** indicates the measurement of the phase difference seen in the early part of these two dicharges, observed from two Mirnov coils located 45 deg apart [**?**]. In #31 the observed phase difference, 0.3 radians, may correspond to an m=17 or 25 toroidal mode. Additionally the power spectrum (for example for #31 at t=2.9 s) displays a f^{-3} decay and exhibits a local peak at 40

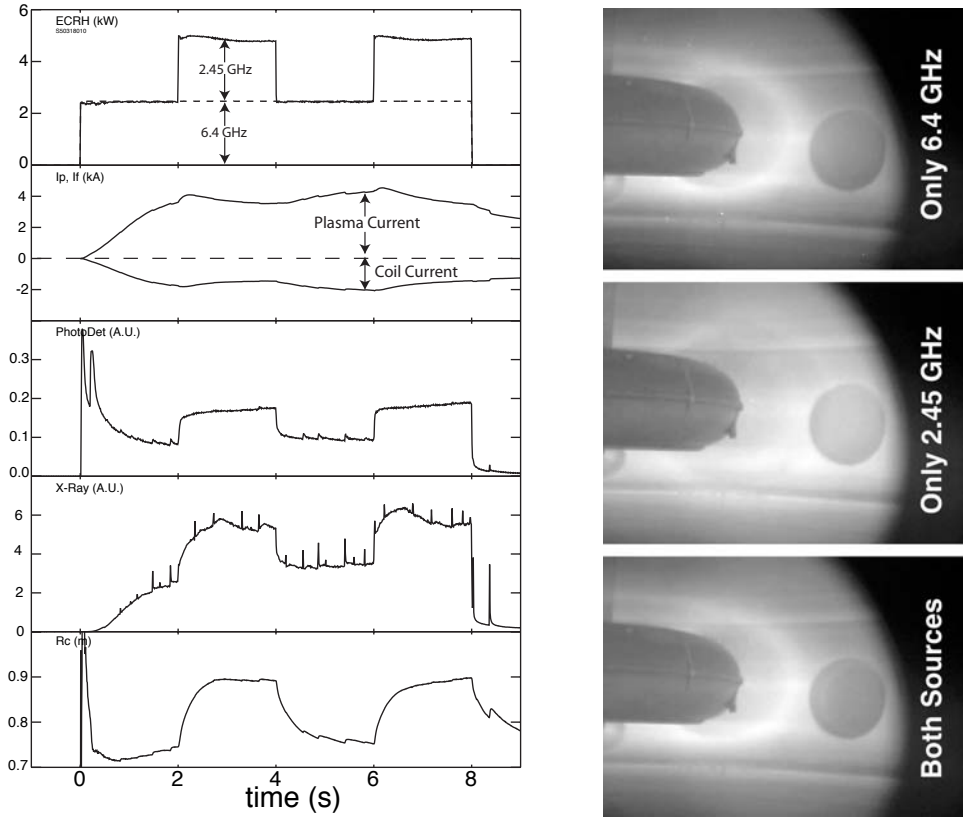

Figure 13: (Left) Illustration of plasma pressure control during modulated multifrequency ECRH. As the 2.45 GHz heating source was switched on and off, the plasma ring current centroid location expanded by nearly 0.15 m. (Right) Visible light photographs at fixed 2.5 kW during the high-beta regime as the microwave frequency changed.

kHz, possibly an indication of MHD activity.

Figure **??** shows several time-frequency domain plots obtained from a multi-cord visible light array that views the midplane of a discharge in which both 2.45 and 6.4 GHz heating was applied. The 6.4 GHz resonance zone is tangent with cord #9 whereas the 2.45 is tangent with core #11. Cord # 9 will therefore view both the 6.4 and the 2.45 heating zone while #11 will only view the 2.45 heating zone. The very low frequencies observed may be indicative of the background plasma confinement, which is low due to rapid losses to the internal coil and its supports. The 6.4 GHz resonance is very close to the internal coil and therefore plasma can be lost faster, which accounts for the higher observed frequency. This observation supports the possibility of a "breather-mode" during ECRH heating.

3.4 Testing Plasma Profile Control with ECRH

Since electron cyclotron resonance heating (ECRH) will deposit power on the resonant mod-B surface, multiple-frequency ECRH can be used to adjust the plasma pressure profile. Demonstrating this capability is an important objective since it will allow systematic study of the relationship between plasma stability and transport and the pressure profile. In our experiments to date, we have launched microwaves with X-mode polarization from locations close to the outer midplane. Ray tracing simulations indicate that the microwaves are weakly absorbed and reflect several times

from the metallic surfaces within the vacuum vessel. The vacuum chamber acts like a very high order reflecting cavity that randomizes the microwave polarization and allows the microwave power to be absorbed with approximate uniformity across the ellipsoidal resonant surface [71]. Although heating at the fundamental is only strong for the X-mode when it approaches the resonance from the high field side [71], waves that reflect from the internal coil and waves that reflect from the top of the vacuum vessel and tunnel through the right hand cut-off into the vicinity of the internal coil will approach the fundamental resonance from the high field side.

When the resonant mod-B surfaces are tangent to field lines on the dipole equatorial midplane, cyclotron heating causes the perpendicular energy to increase rapidly to form energetic trapped electrons. The fundamental resonances for the 6.4 and 2.45 GHz sources cross the midplane at $r =$ 0.59 and 0.76 m respectively. Since the floating-coil limiter is located at $r = 0.57$ m, fundamental cyclotron heating with 6.4 GHz is not likely to be a significant producer of energetic trapped electrons. Instead, as the electron temperature increases, the harmonic resonance of the 6.4 GHz microwaves, located at $r = 0.71$ m, probably contributes most to hot electron heating.

We have demonstrated control of the location of the plasma ring current centroid by modulating the power levels of multi-frequency ECRH sources. Fig. 13 displays a discharge that was heated for 8 s with 6.4 GHz microwaves and a periodic application of 2.45 GHz heating power. Since the fundamental resonance for 6.4 GHz is located at $r = 0.59$ m (and is close to the floating coil limiter at $r = 0.57$ m), the initial location of the plasma current centroid is calculated to be $0.72 < r < 0.75$ m, and this may reflect heating at the harmonic resonance. As the 2.45 GHz power is switched on, the ring current expands outwards approximately 0.15 m. Additionally, video recordings of the visible light indicate a broadening of the light "halo" during the high-beta regime during 2.45 GHz as is expected for microwaves that deposit power at a greater distance from the floating coil.

3.5 Investigation of Plasma Shape and Compressibility

In order to investigate the coupling between the edge plasma and the hot plasma core within a dipole-confined plasma as well as to observe the difference between limited and diverted plasmas, low-current copper coils which shape the outer flux surfaces have been located at the outside of the vacuum vessel. By energizing the shaping coils with respective currents I_{h1} and I_{h2}, $-50 < I_{h1}, I_{h2} < 50$ kAT, the position of the ring null divertor can be positioned from the outer vacuum chamber wall ($R_w = 2.5$ m) to a midplane radius of 1.2 m. The coils form a Helmholtz pair so that, for balanced currents, they will not significantly alter the stability of the floating coil during levitation.

Three examples of LDX equilibria for an edge pressure of p_{sol} =0.25 Pa are shown in Fig. 14. For low currents, $I_h < 5$ kAT the confined plasma flux remains limited at the outer midplane. As the Helmholtz coil current increases, $5 < I_h < 12$ kAT a separatrix forms with two X-points located above and below the midplane, leading to an increase in $V = \oint d\ell/B$ as a consequence of the vanishing magnetic field strength in the vicinity of the X-points. Above 15 kAT the two X-points coalesce into one on-axis X-point (Fig. 14) and V near the separatrix decreases as the Helmholtz current increases.

Preliminary experiments were performed to investigate the relationship between plasma shape and the first stage LDX plasma discharges. In these experiments, the shaping coils were operated as a balanced Helmholtz pair, and the current was systematically raised to 32 kAT. We observed that, for a fixed neutral gas pressure of sufficient level to transition to the high-beta regime, the plasma diamagnetic current (approximately proportional to the plasma stored energy) did not change for moderate levels of Helmholtz current, I_h. We observed that the stability of the hot electrons was not affected by plasma shape and the hot electron pressure (measured in the high beta regime)

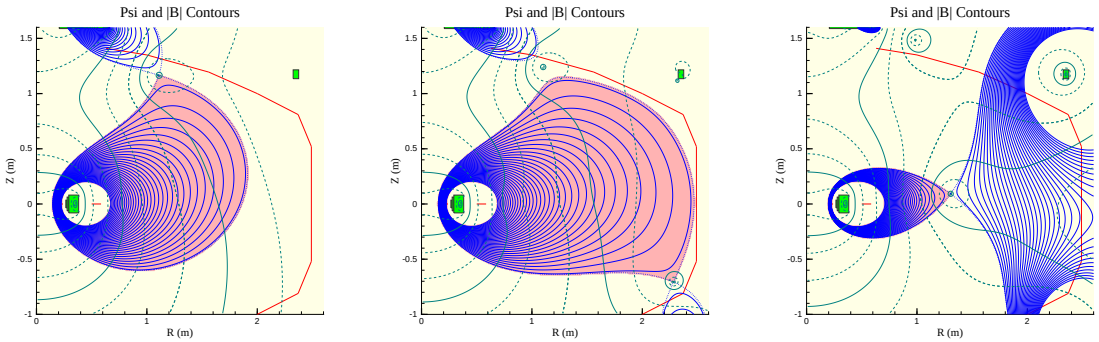

Figure 14: Examples of diverted LDX equilibria: (A) Shaping coils off, (B) Shaped for maximum plasma volume and β, (C) Shaped for small plasma volume.

remained constant. However, when I_h exceeded a critical value, dependent upon the neutral fueling rate, high-beta plasma could not be sustained and the HEI mode caused a rapid transition back into the unstable low density regime.

We have considered several explanations for the reduced stability at high values of I_h. One possibility is that smaller plasmas created at high I_h increase the hot electron density gradient. However, we observe the hot electron density to be highly localized near the equatorial cyclotron resonance and far from the outer plasma boundary. Furthermore, stable hot electron populations occur during the afterglow when the hot electron density gradient further steepens. Another possibility is that the background plasma in the vicinity of the hot electron population is reduced. The cold background plasma likely has an MHD-like behavior and stability is determined by the compressibility constraint, $\delta(pV^\gamma) > 0$. MHD fluctuations could drive plasma convection and give rise to a central peaking (Eq. 3) of the background plasma that is proportional to the flux expansion between the edge and plasma core locations. As a result, as the separatrix moves inwards and the flux expansion decreases with a fixed edge density the cold plasma density in the hot core would be reduced. When the cold density falls below a critical value it will destabilize the hot electron interchange mode.

Both the cold plasma fraction and the hot electron gradient determine the HEI instability threshold and both evolve in a way that is consistent with the observation that at a critical shaping coil current the plasma becomes unstable and drops back into the low density regime. However, because strong density peaking is observed in stable plasmas during the afterglow, we believe the second possibility to be the more likely explanation. As such, the decreased hot electron stability at high I_h would constitute our first direct observation of the beneficial role of large-scale plasma compressibility. Shaping investigations continue to be an active research topic, and new experiments are planned to improve our understanding of the dependence of plasma stability on shaping and flux expansion.

4 Proposed Research

This renewal proposal requests funds to carry out a four-year scientific study made possible by the construction of the new LDX research facility. For the first time, we will be able to evaluate

the confinement and beta limits of a levitated dipole configuration and to study the processes that would regulate the cross-field transport of a fusion-relevant configuration.

The proposed research plan builds upon the successful first-stage investigations of the dipole confinement concept that have used a supported coil. In particular, we have learned how to create, sustain, and diagnose high-beta dipole plasmas, demonstrated the use of neutral gas fueling to control plasma density and to stabilize instabilities, demonstrated simple plasma profile control using multiple-frequency ECRH, and identified a variety of plasma dynamical processes that will guide our future investigations of plasma transport and control. Up to the present we have operated in the supported mode. We expect that the comparison between the supported and the levitated mode will provide valuable information on the value of internal coil levitation for producing fusion grade plasmas

Our proposed research plan follows the next three operational stages as originally planned for the LDX Project. These next stages are: (ii) levitated coil operation and investigation of dipole confinement and stability in high-temperature plasma, (iii) investigations of high-density plasma created with fast-gas injection, Li-pellet injection, and high-frequency (28 GHz) gryotron heating, and (iv) experiments with high-density plasma heating in order to investigate the energy confinement properties relevant to projected fusion power regimes.

Because our new experiments will be conducted when the floating coil is magnetically levitated, we will begin exploration of a fundamentally new regime of dipole plasma confinement. As described in the previous section, plasmas confined by a supported coil were limited either by rapid losses induced by instability during the "low density" regime or by heat conduction to the three radial supports during the "high beta" and "afterglow" regimes. While we have learned to control the hot electron interchange instability with programmed gas control, the thermal and particle losses to the support rods will only be eliminated by levitated coil operation.

We expect that the stored energy in the high beta regime will increase substantially when we eliminate plasma losses along the field lines. By eliminating the loss-cone for hot electrons that circulate through the floating coil, we will also obtain a more isotropic plasma pressure. The LDX research plan is organized along two interconnected pathways: the scientific tasks and the facility stages that allow for the safe and reliable operation of the LDX superconducting magnets and that allow for the coordinate installation and test of diagnostics and research tools.

The scientific goals of the research plan can be summarized by the following tasks:

- To test and understand the stability of high beta plasmas in a dipole field.
- To measure and control particle circulation and adiabatic heating.
- To measure and understand dipole plasma confinement at high beta.

These tasks are interrelated, and the experimental "campaigns" will overlap in time and produce data that will be integrated to form an overall assessment of dipole plasma confinement at high beta. Each of these physics tasks involve active experiments where plasma control tools (*e.g.* shaping coils, multiple frequency electron cyclotron heating, and high-density particle and heating sources) are used to modify plasma conditions and where plasma diagnostics are used to measure local and global parameters. These physics tasks are strongly coupled to our theory and modeling efforts.

The first of our four-stage facility plan began in August 2004 with the start of physics experiments using a supported coil. The proposed four-year LDX schedule provides for the levitated coil operational phases and allows experimentation with both long-pulse, energetic electron plasmas produced by ECRH and for the experimental study of higher density plasma using a variety of relatively low-cost pulsed fueling and heating sources.

The second stage will begin early in the first year of our proposed program when we will conduct the first plasma experiments with a levitated coil. At this stage we will begin to evaluate the expected improvement in plasma confinement that results from the elimination of the coil support rods in the context of the scientific tasks listed above. Our scientific experiments will focus on the demonstration of compressibility stabilization through the systematic variation of plasma shape, the initial investigations of the role of weak magnetic shear, and the maximization of stored energy by using multiple frequency ECRH.

The third stage in our facility plan involves the study of the confinement of high density plasmas where the effects of energetic electrons are reduced and plasma dynamics dominated by better "thermalized" and more "MHD-like" plasmas can be studied. The final stage of the facility plan explores the energy confinement of high-density plasmas that are heated with a pulsed, relatively low-cost, power source.

We believe the proposed program plan meets our overall objective for the LDX project: to test whether fusion can benefit from nature's way to magnetically confined high-pressure plasma. At the end of the proposed four-year program, we anticipate a significant advance in the understanding of the equilibrium, stability, and confinement properties for a plasma that is confined by a levitated dipole. LDX will also provide the basis for understanding of (1) the confinement and stability of plasmas containing energetic particles, (2) the relation between edge plasma and a hot plasma core, (3) the possible elimination of drift-wave turbulence to produce plasmas with classical confinement, and (4) the circulation and adiabatic heating of plasma confined by closed, shear-free magnetic field lines and by toroidal magnetic fields with weak magnetic shear.

4.1 Detailed Research Plan

This section describes the research plan that fulfills the scientific objectives of the LDX program. The experimental plan describes a series of experiments performed in the levitated configuration that investigates the stability and confinement properties of a levitated dipole. Physics themes present throughout our research are the importance of pressure and density profiles, understanding edge parameters, and the important role of plasma density.

Control Tools and Diagnostics

Compared to the facility and fabrication work that was necessary to fabricate our three superconducting magnets during the previous grant period, there will be less facility work and fewer and simpler installations during the proposed grant period.

At the start of this renewal proposal period, supported-coil experiments will end, and we will begin the levitation phase. Our existing catcher was designed to remain in contact with the floating coil. The "stage-two" catcher has been designed and it will replace the existing catcher and allow lift-off and gentle landing of the floating coil onto the pneumatic launcher system. At the time of the writing of this proposal, we have already begun the hardware tests and final installations that will be used to levitate the floating coil. These tasks include (i) the integrated full current operation of all three superconducting magnets (now underway), (ii) the installation of the lower catcher fixture and upper catcher frame shown in Fig. 15, (iii) the installation of the eight-channel, redundant, laser detection and position control system and (iv) the integrated tests of our existing realtime levitation control system. The operation of the real-time digital control system has been successfully tested with a permanent magnet and the laser detection system has been designed. Since all of the LDX magnets and control systems can operate when the vacuum chamber is vented, we plan a one-to-three month period where floating coil levitation is demonstrated without plasma (and with

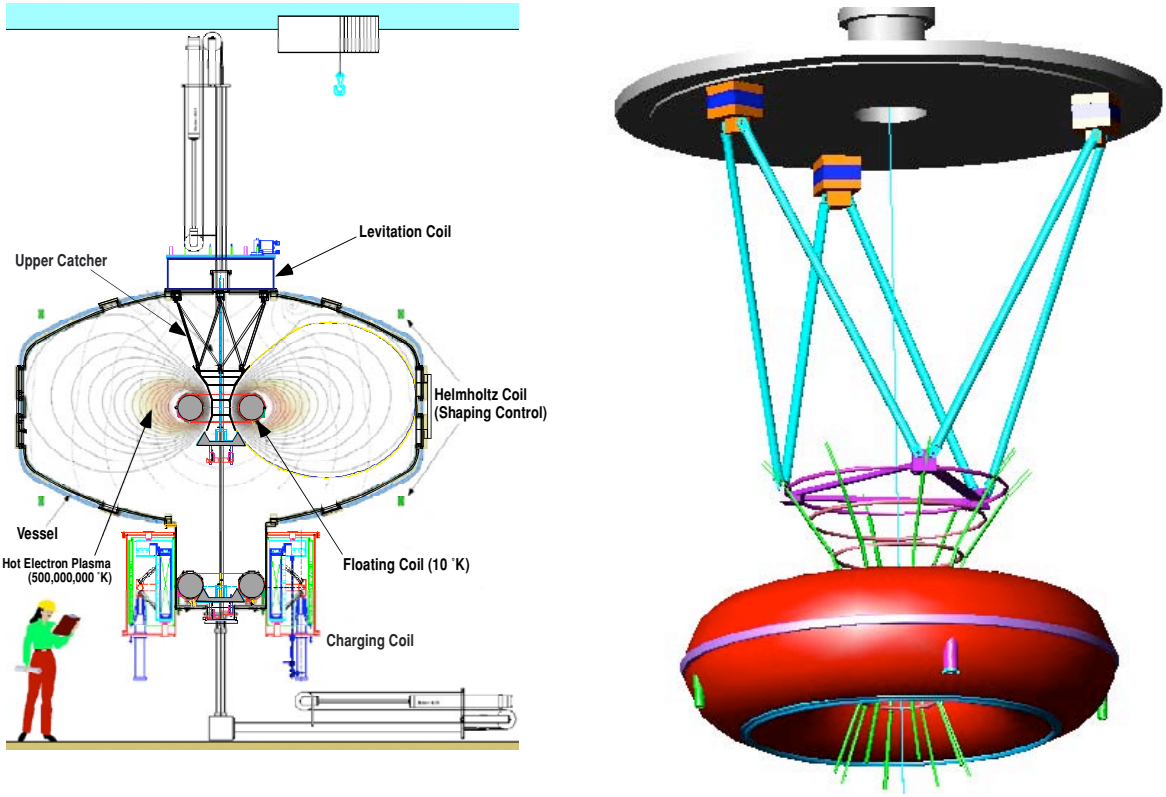

Figure 15: (Left) Cross-section of the LDX experiment configured for levitated operation, and (right) a schematic of the upper catcher showing the support structure that will be used for near-plasma magnetic diagnostics and possible low-power, slow-wave ICRH antenna.

supplemental safety restraints.) The first plasma experiments with a levitated coil will occur in the fall of 2005.

We have designed LDX to permit a substantial versatility in plasma studies. The control knobs utilized in the initial experiments described in Sec. 3.2 include the following:

- Multiple frequency ECRH. We have heated the plasmas using two frequencies (2.45 and 6.4 GHz) and observed an ability to vary the pressure profile.
- Programmable gas feed. It has been observed in many different configurations that the level of gas fueling will determine the stability of an ECRH plasma. We have developed a gas system that permits a temporal programming of the gas fueling rate and permits easy variation of the gas species.
- Shaping coils. We have incorporated into the facility a pair of coils in a Helmholtz arrangement that permits a large variation of the plasma shape and flux expansion as shown in Fig. 14. This gives LDX the capability of scanning from a limited to a diverted configuration and of varying the stabilizing compressibility term.

Installation of additional control tools are staged to coincide with important experimental levitated operational campaigns. In the proposed research period we will add the following controls:

- Additional ECRF heating sources at 10.5, 18 and 28 GHz.
- Fast-gas nozzles for efficient and rapid fueling and impurity injection.
- Application of a weak toroidal field in the plasma by imposing a current in the center post so as to create flux surfaces and thereby change the MHD properties of the configuration.
- Edge bias probes to drive and control large-scale plasma convection for transport and adiabatic heating studies
- A low-cost Li-pellet injector to create and study the spatial homogenization of large density sources
- A low-cost, pulsed plasma heating source ($\sim$ 100 kW) in order to investigate energy confinement and confinement scaling of plasma with density exceeding the cut-off frequencies of our microwave sources.

In addition to the basic diagnostic set discussed in Sec 3.2 the following diagnostics will be added:

- A multi-cord microwave interferometry will be used to measure the density and estimate the density profile. The first cord has been installed and operates at 60 GHz with a superheterodyne receiver.
- An optical spectroscopy detector array will be installed in order to measure impurity and plasma convection.
- A multi-cord doppler spectrometer will be installed. We plan to make use of the novel, high-throughput line-spectrometer developed by S. Paul [82] that uses interference line filters.
- A neutral particle energy analyzer will be installed midway through the proposed project year to measure T_i in high-density plasma.

4.1.1 Understanding and Controlling Density in LDX

Plasma density plays an important role in the LDX experiment since microwave electron cyclotron resonance heating (ECRH) is used to form and heat the plasma. Based on early LDX experiments as well as on extensive experience with ECRH in magnetic mirrors, tandem mirrors, bumpy tori, and in the CTX device, plasma density is known to be a critical operational parameter. Besides microwave accessibility, plasma density regulates the intensity of relativistic electrons. When the neutral pressure is either too large or too small, the density and temperature of trapped energetic electrons decreases. In LDX, the plasma density is controlled by precisely pre-programming neutral gas puffs. Later, high-speed, fast-acting gas puffs, inner gas fueling, pellets, and edge plasma sources will be explored as techniques for density control.

We expect the rate of gas fueling that optimizes the production of energetic electrons and electron stored energy will be less during levitated operation than during supported operation. This is because levitated operation will eliminate loss of cool plasma to supports and particle recycling that occurs on a pitch-angle collision time. During levitated operation, we also eliminate the loss of hot electrons due to pitch angle scatter on neutrals or anisotropy driven instability. While proper adjustment of gas fueling has been important in the supported coil experiments, the investigation of density and neutral gas control will become even more important during operation with a levitated coil. The well-confined plasma in a levitated dipole will likely be a better particle "pump" requiring

reductions in the deuterium gas feed and operating pressures as compared with CTX experience. The care we have given to the quality of our vacuum chamber (base pressure $< 10^{-8}$ Torr) will help insure that the plasma density doesn't "run away" during levitated operation. The reduced end losses should also increase the temperature of the warm (non-relativistic) electrons, further enhance the rate of hot electron production, and significantly increase the already substantial plasma pressure.

As discussed in Section 3.1.1, the stability limits for high-pressure dipole-confined plasma will differ depending on whether the pressure is contained in the energetic electrons or in a thermalized, high-density plasma. Energetic electrons neutralized by colder ions are subject to the kinetic HEI instability and have stable pressure gradients that can exceed the MHD compressibility criterion. The cooler background density, however, necessary for stabilization of the HEI is expected to behave in a MHD manner, including the generation of convective cells. The non-thermal electrons have rapid magnetic drifts that may influence convective cells and the symmetry of any electrostatic and density structures that may form in a dipole.

For a thermal dipole plasma operating at the MHD stability limit the adiabatic pressure ratio limits the peak pressure, p_0, to a value set by the scrape-off layer pressure, p_{sol} *i.e.* for the largest flux expansion envisioned for LDX, $p_0/p_{sol} \sim (V_{sol}/V_0)^{\gamma} \sim 5000$. Following theoretical results [29, 24] we anticipate that a sufficiently dense plasma will behave in a manner consistent with MHD: for sufficiently strong heating the plasma will encounter the stability limit and large scale convective flows will form. At equilibrium there must be a flow of power from the plasma core to the scrape-off-layer that is equal to the heating power of the plasma (less radiation losses). In other words the energy confinement time will adjust so that the energy flowing within the scrape-off layer and into the wall becomes equal to the net heating power. Assuming that a fraction, f_R, of power leaving the plasma is radiated, we can write a power balance:

$$\frac{(1 - f_R) \oint p dV}{\tau_E} \approx 2 p_{sol} A_{sol} c_s \tag{4}$$

with c_s the scrape-off layer sound speed, p_{sol} the scrape-off layer pressure and A_{sol} the scrape-off layer cross-section area. We will assume that the minimum width of the scrape-off layer is an ion gyroradii and take $A_{sol} \geq A_{min} \approx 2\pi R_{sol} \rho_{sol}$ with ρ_{sol} the scrape-off layer ion gyro-radius at the outer radius of the scrape-off layer. We will define $\tau_E(A_{sol} = A_{min}) = \tau_E^{crit}$. The scrape-off layer pressure, p_{sol} is obtained assuming $p \propto V^{-\gamma}$.

When heating is applied to the core plasma and $\tau_E = \tau_E^{crit}$, sufficient energy and particles are supplied to the scrape-off layer to form a marginally stable equilibrium. When $\tau_E < \tau_E^{crit}$, there is more energy entering the scrape-off layer than can be accommodated and it is expected that the scrape-off layer will expand to accommodate a higher heat flow. However τ_E cannot exceed τ_E^{crit} because the peak pressure relative to the scrape-off layer is limited by the MHD interchange condition and the energy outflow must maintain the scrape-off layer (the scrape-off layer cannot be narrower than an ion gyroradius). Convective and turbulent processes are expected to prevent τ_E from exceeding τ_E^{crit}.

The hot electron plasma parameters may be assumed to be substantially better for the floating coil than the supported coil results. (In the University of Tokyo Mini-RT experiment [45] an order of magnitude improvement in plasma pressure was found when the internal coil was floated).

- For an optimized hot electron plasma we anticipate $T_{eh} \gtrsim 100$ keV, $n_{eh} \approx 3 \times 10^{16}\ m^{-3}$, $\beta_h \approx 0.55$ and with the pressure peak located at $R_0 = 0.76$ m, and $R_{sol} = 2.5$ m.

- For such a plasma assume that we rapidly increase the density and transfer half of the stored energy to the now denser thermal plasma. If the core density rises to $n = 1 \times 10^{19}\ m^{-3}$ at

$\beta \approx 0.27$, then we would obtain $T_{i0} = T_{e0} = 240$ eV. If we further assume that radiation is insignificant ($f_R \sim 0$), we obtain from Eq. 4 an estimate for the critical energy confinement time, $\tau_E^{crit} = 130$ ms.

Since these parameters are consistent with computed free-boundary equilibria and MHD stability [2], they provide useful targets for our experiments, and they have guided selection of diagnostics and the order of our research plan.

4.1.2 Understanding Compressibility and Stability at High Beta

A major objective of the LDX experiment is to provide the first systematic investigation of the use of MHD compressibility to stabilize large pressure gradients in a high-temperature and high-beta plasma. As explained above, for stabilization by compressibility, MHD requires that the pressure gradient satisfy the adiabaticity condition, $\delta(pV^\gamma) < 0$. Thus, for a MHD plasma, the maximum beta and plasma stored energy occurs when the pressure gradient is nearly marginal from the hot core to the edge, when the flux-tube volume ratio, V_{sol}/V_0, is large, and when the edge pressure is significant. The goal of our investigation of compressibility stabilization is to understand the relationship between plasma stored energy, the pressure profile, the shape of the outer boundary, and the edge plasma.

In a ECRF heated plasma with a hot electron component the background plasma is expected to behave in a MHD-like manner. In early experiments we will observe the effect of compressibility on the background plasma and in later, high density experiments we expect compressibility to determine the stability of the high beta thermal plasma. Thus the most important experiments will be carried out in thermal plasmas.

Our compressibility experiments involve three elements:

1. Measurement of the pressure profile and stored energy by reconstructing the plasma equilibrium from measurements of the magnetic flux, local field and by direct measurement of the edge plasma with movable probes.

2. The use of multiple ECRH heating frequencies to modify the pressure profile.

3. Systematically change the compressibility parameter by imposing large variations of the plasma shape by energizing the Helmholtz coils and causing significant changes in the flux-tube volume, V_{sol}/V_0.

The demonstration of plasma compressibility will follow clearly from the ability to show that we can reach a critical pressure profile and therefore a critical peak pressure that depends upon the ratio of V_{sol}/V_0. As shown in Fig. 14 we are able to change this ratio significantly. From MHD the peak pressure, stored energy, and plasma diamagnetic current can be expected to change by more than a factor of 30 (and $\langle\beta\rangle$ changes even more) as the Helmholtz coils are energized reducing V_{sol}/V_0 for a marginally stable pressure profile .

The pressure profile and stored energy will be measured through reconstructions from magnetic measurements: 8 flux loops and 18 Hall probes and pick-up coils. When an energetic electron component is present our x-ray imaging camera and interferometer array will lend support to the magnetic reconstruction. The comparison of the critical pressure gradient with the MHD interchange criterion will elucidate the limits of compressibility stabilization.

Multiple frequency electron cyclotron heating will be used to adjust the plasma pressure profile. Langmuir probe measurements will permit direct measurements of the scrape-off layer characteristics. Fluctuations of the magnetics data will detect MHD instability.

4.1.3 Particle Circulation and Adiabatic Heating

Unlike toroidal plasma confined by nested magnetic surfaces that have magnetic shear, the dipole field permits rapid, adiabatic particle circulation that may make the dipole concept ideally suited to utilize advanced fuels in a fusion power source [32]. As discussed in Section 3, a fundamental property of magnetic topologies with closed field lines lies is the tendency of the field lines to charge up and generate large scale $\mathbf{E} \times \mathbf{B}$ convective flows. Rapid particle circulation and adiabatic heating exists within Earth's magnetosphere. In the outer regions of the LDX plasma, this process is expected to impose a stiff limit on the pressure gradient, forcing the profile to be near the critical gradient predicted by ideal MHD interchange theory. Although particle circulation may be rapid, convective flows do not necessarily give rise to energy transport. Showing the existence of these flows within the laboratory is a critical part of our evaluation of the feasibility of the dipole configuration as a fusion concept.

Although convective cells can form in the cold background plasma of hot electron plasmas they would not directly affect the rapidly drifting hot electron component which is responsible for the plasma pressure. Studies of convective cell will begin in the second year of this proposal to measure large scale convection in the background plasma. Studies of convection in the high pressure thermal plasmas will be carried out during the third and forth year of the proposed research program.

In our investigations of large-scale convective cells and the axisymmetry of the electrostatic potential profiles we will focus three active approaches. First, we will measure convection and the rate of circulation of impurities that move from the edge to the core following a short and spatially-localized impurity "spark". The impurity flow patterns and resulting averaged inward impurity flux will be observed spectroscopically. Secondly, the symmetry of the electrostatic potential will be measured with probe arrays at the plasma edge. Finally, movable emissive probes will be used to measure the time-variation of the electrostatic potential at a particular toroidal location. We will also investigate their use to excite convective cells by modulating their bias.

Once we have successfully identified convective cells and measured the rate of inward particle convection, three other experiments will be conducted to further understand the formation of convective cells. These are:

i. The eight TSR saddle coils will be used to generate (and eliminate) small magnetic field errors that may cause stationary ambipolar potentials.

ii. Up to 4 kA will be driven through the launcher cables to create a weak toroidal field (10-20 G) and permit a test of the suppression of convective cells with magnetic shear [34].

iii. The Lithium pellet injector, installed for transient density studies in the third year, will most likely create large, localized, and easy-to-measure density perturbations that will create large $\mathbf{E} \times \mathbf{B}$ convective flows.

4.1.4 Understanding the Effects of Weak Magnetic Shear

The LDX device is the world's only high-beta, quasi-steady state, toroidal confinement device without magnetic shear. The addition of a toroidal field may help to smooth nonsymmetric plasma heating [42], reduce the effects of field errors [8], and prevent inward convection to the floating ring. Since the pulsed application of a weak magnetic field is relatively easy to perform, we propose to insulate the launcher apparatus and energize an axial conductor with currents in excess of 5 kA. The return currents would be conducted through cables located along the vacuum vessel, and the toroidal field current pulse would probably be generated with an electrolytic capacitor bank and

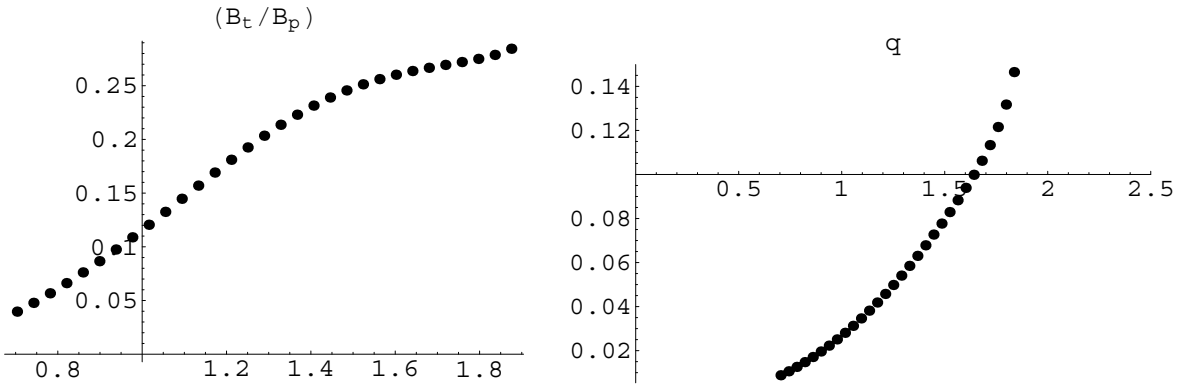

Figure 16: Free-boundary equilibrium profiles for a high-beta LDX equilibrium with a weak toroidal field. (Left) The ratio of the toroidal field to the poloidal field along the outer equatorial plane, and (Right) the safety factor profile.

power crowbar. A bank energy of 5 kJ would be sufficient to energize the conductor to more than 25 kA,

We have computed free-boundary equilibria for LDX in the presence of a toroidal magnetic field. When equilibria are computed numerically, the (unrealistic) restriction on the form of the toroidal flux used by Catto and Krasheninnikov [42] is unnecessary. In particular, three types of LDX equilibria with a toroidal field have been studied: (i) fully relaxed equilibria with a toroidal field produced from a central conductor, (ii) inductive equilibria where poloidal currents in the plasma are induced by a time-varying current a central conductor, and (iii) equilibria where the poloidal currents are sustained by local current drive. It is perhaps not surprising to note that (because the current within the floating ring is very large, ~ 1.2 MA) the poloidal field structure of LDX equilibria will not change significantly with the addition of a weak toroidal field generated by a few 10's of kA of central or poloidal currents.

Fig. 16 shows profiles from a representative high-beta LDX equilibrium with a weak toridal field. The plasma safety factor profile and of the magnetic field line pitch on the outer equatorial plane are shown. The parameters of the equilibrium are similar to those shown in Fig. 1 and described by Garnier [2]. The volume-averaged beta was $\langle\beta\rangle = 0.32$; peak beta exceeded unity; and the toroidal diamagnetic plasma current was 14.3 kA. The applied axial current was 50 kA and the total poloidal plasma current was 14.7 kA. This level of toroidal field is at least an order of magnitude *larger* than required to suppress small-scale convective cell transports based on the criteria observed in the Wisconsin octupole.

4.1.5 Dipole Confinement Studies

The third scientific objective of the LDX experiment is to provide the basic understanding of energy confinement in a dipole magnetic field and to test conditions that may eliminate drift-wave turbulence and produce plasmas with classical confinement. LDX will enable the first observations and investigations of high-temperature plasma confinement for many collisions times in a large plasma with strong compressibility effects. As discussed in Section 2, when both the pressure profile and the density profile are near adiabatic, theory suggests that electrostatic drift modes are stable. These adiabatic profiles have density profiles that scale with radius as $n(\psi) \sim 1/V(\psi)$ and pressure profiles that scale as $p(\psi) \sim 1/V^{\gamma}$. The gradient parameter, $\eta = d\ln T/d\ln n \sim 2/3$ is a constant. What distinguishes the dipole concept from others is it's large variation in the flux-tube

volume, $V(\psi)$. When the dipole satisfies drift-wave stability criteria, both the pressure and density profiles remain sufficiently steep to be relevant for fusion energy.

Several active experimental studies will be made to investigate dipole confinement beginning with low-density plasmas containing significant energetic electrons and ending with high-density plasma with greatly reduced energetic electron populations. In all cases, we will measure global stored energy, pressure profiles, and the edge plasma. Equilibrium reconstruction using magnetic measurements is the primary diagnostic tool, but we will also use a multicord microwave interferometer to estimate the electron density profile and a neutral particle charge-exchange energy analyzer to indicate the ion temperature.

For plasma with large fractions of energetic electrons, the injected ECRH microwaves are strongly absorbed, and this makes estimations of global confinement times relatively easy. However, the rapid magnetic drifts of the energetic electrons allow pressure gradients to exceed the usual MHD interchange constraint. For energetic electron plasma, the global energy confinement times can be larger than the critical values, τ_E^{crit}, that balance scrape-off layer losses. For these plasmas, our confinement studies will emphasize edge plasma measurements, edge fluctuations, and maximizing the total stored energy by adjusting the pressure profile with multiple frequency ECRH.

Perhaps, our most important confinement studies will occur upon study of high-density thermal plasmas. It is with these plasmas that we will seek to create conditions that meet the dual adiabaticity constraints on (thermal) pressure and density. Our goal is to create high-beta plasma with large variations in the η profile parameter: ranging from peaked density to hollow. When $\eta \approx 2/3$, the profile should remain stable to drift-wave turbulence and simultaneously maximize energy confinement.

As already mentioned, modifications to the density profile will be made by fast gas injection, both from the edge and from the floating coil, and by pellet injection. Additionally, the plasma may "naturally" adjust its profile towards the condition $\eta \approx 2/3$ due to particle circulation and adiabatic heating. High density experiments with different shapes (*i.e.* compressibility parameters, V_{sol}/V_0) will also be investigated.

While these experiments will focus on understanding the relationship between profiles and confinement, this research phase of the LDX program will also investigation techniques to increase plasma pressure and energy confinement and global performance.

4.1.6 Pulsed Plasma Heating to Investigate Energy Confinement

As we attempt studies of higher density dipole-confined plasma, we expect to be limited by the available power of our 28 GHz gryotron. In order to investigate energy confinement of high-density plasma, we intend to specify and install a relatively low-cost heating system that can be effective above the cut-off density for our microwave heating sources.

The requirements for this heating system are: (i) approximately 100 kW of injected power, (ii) at least 20 ms heating pulses, (iii) compatible with our existing research facility, (iv) relatively low cost, and (v) relatively easy operation. We've considered two options.

The first high-density heating option is to purchase a diagnostic neutral beam from the Budker Institute of Nuclear Physics (Novosibirsk, Russia) similar to the DNB used by the MST experiment [81] for the measurement of Rutherford scattering, charge-exchange recombination spectroscopy, and internal magnetic field measurement using the motional Stark effect. The LDX neutral beam would inject 4 A of 20 keV protons for 20 ms. The beam would be injected horizontally and aimed at the peak of the plasma density. Protons would be injected instead of deuterium in order to minimize ion orbit effects. When the peak density of the target plasma reaches 10^{19} m^{-3}, only a

small fraction ($\sim 25\%$) of the beam energy passes through the plasma. An advantage of purchasing and installing a low-power beam heating system will be its possible diagnostic uses.

The second option is to design and install an ICRF heating system. An attractive design now under consideration is to locate a slow-wave launching system on the upper catcher frame and launch 4-5 MHz slow waves in a "magnetic beach" configuration. This high-density RF heating system has the advantage over fast-wave heating if only because the size and inductance of the launching antenna can be made small in order to minimize the antenna voltages.

At the moment, neither of these design options are fully designed nor have we established the plasma target conditions that would warrant their installation. Nevertheless, during the next four years of our research plan, we expect our near-term technical objectives to be achieved on schedule. After the installation of the complete multifrequency ECRH system and the fast gas and density control systems, it is highly likely that additional heating sources will be needed in order to properly investigate dipole energy confinement. The low-power DNB and ICRF systems appear to be feasible, and we intend to prepare detailed specifications of these systems within a two-year time frame.

4.1.7 Advanced Studies

We list here plans for several "advanced studies" of dipole physics that may be investigated during the end of the proposed project period. These include:

- The use of an array of edge probes or an axisymmetric limiter to create an axisymmetric radial electric field and excite axisymmetric rotational flows. We would test whether these flows might create an edge pressure pedestal.
- The design and configuration of advanced diagnostics such as a heavy ion beam probe to measure the internal plasma potential and structure of convective cells.
- The possibility of preferential removal of chosen species as they convect toward the outer region of the confined plasma region, possibly by the use of localized ion cyclotron heating.
- The investigation of bottom levitation and the specification of the required enhancements to our feedback system. Bottom levitation produces the point-null configuration that may aid in the understanding of scrape-off layer parameters and reduce charge-exchange losses.

4.2 Project Schedules and Milestones

Figure 17 presents an overview of the schedule for LDX experiments and operations. The proposed research plan begins with the conclusion of experiments with a supported coil, and is divided into two phases: (1) experiments with a levitated coil (2) experiments with higher-density plasmas. The four-year schedule sets a relatively rapid pace of scientific investigation. We believe this is appropriate for the first study of a new concept. Our strategy is to conduct active experiments that reveal limiting processes within LDX dipole-confined plasma and that determine gross (and relatively easy-to-measure) features of high-beta stability, confinement, and particle circulation. The installation of new microwave heating and density control tools are staged throughout the next four years so that important physics can be understood as new capabilities become available. We expect some interesting scientific surprises, and, for this reason, we anticipate that most investigations will span more than one program year. Many will become the subjects of doctoral dissertations.

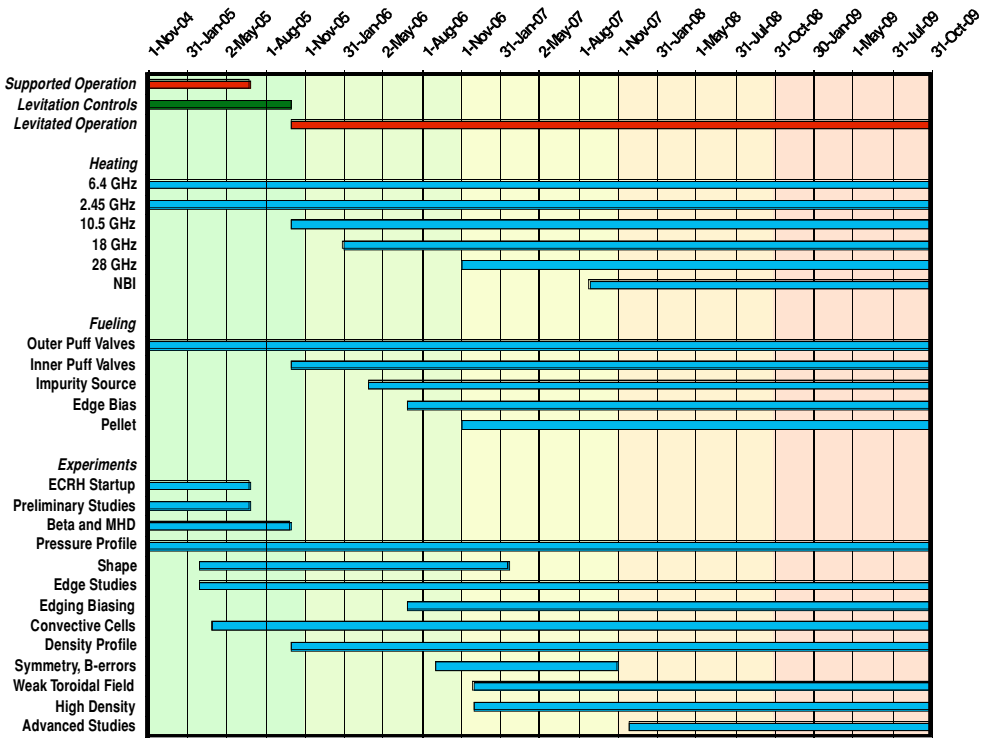

Figure 17: Overview of the proposed four-year schedule of LDX experiments and operations.

4.3 Statement of Work and Deliverables

Our proposed LDX research program will answer two important questions needed to establish the dipole fusion concept and achieve several research objectives that advance our fundamental understanding of dipole physics.

- First, LDX will answer the question: can a dipole magnetic field confine a high beta plasma with near classical energy confinement as suggested by theory?
- Second, experiments with LDX will determine whether plasma confined by a dipole can circulate rapidly from the core to the edge without degrading energy confinement.

The answers to these two questions are necessary to evaluate the suitability of the dipole fusion concept to burn advanced fusion fuels.

Our LDX experimental program will also advance our fundamental understanding of several important areas of plasma physics and magnetic fusion science. These include:

- The study of high beta plasma stabilized by compressibility. The compressibility constraint will determine the coupling of the scrape-off-layer and the hot plasma core.
- The determination of the relationship between drift-stationary profiles having absolute interchange stability and the elimination of drift-wave turbulence.
- The investigation of strong plasma flows and convective cells in a large confined plasma without magnetic shear.

- The understanding of the stability and dynamics of high-beta, energetic particles in dipolar magnetic fields.

By the end of the proposed research program, we will have had four years of systematic study of high beta dipole plasmas and be able to report on the feasibility of the dipole confinement concept as a potential route to an innovative fusion power source. These studies significantly benefit from especially strong interactions with theory and modeling efforts.

Figure 17 also shows the schedule for the installation and operation of equipment and the experimental facility. The installation of new equipment is staged to coincide with needs in the scientific program. In this section, we have list the major installation and facility tasks planned for the next four years. These tasks are fewer and much simpler than those associated with the fabrication of our three superconducting magnets. When completed, they provide all of the research tools required for our physics objectives.

- Year 1: November 2005 – October 2006
  - Purchase impurity spectrometer and imaging diagnostic.
  - Install additional cords for microwave interferometry.
  - Install gas valve near floating coil to be used to alter density profile
  - Install waveguide and utilities for existing 10.5 GHz and 18 GHz klystrons used for pressure profile control experiments.
- Year 2: November 2006– October 2007
  - Install impurity "spark" source.
  - Install neutral particle charge-exchange energy analyzer.
  - Install and test edge bias probes to induce electrostatic particle convection.
  - Install waveguide and utilities for (existing) 28 GHz gyrotron operation.
- Year 3: November 2007 – October 2008
  - Install Li pellet injector.
  - Install Neutral beam and/or ICRF heating.
- Year 4: November 2008 – October 2009
  - Upgrade diagnostics and perform high density and high power experiments.

4.4 Educational and Outreach Activities

As a new experiment in the U.S. fusion program, LDX has an important educational and outreach goal. The LDX experiments are closely related to the physics of magnetospheric plasma, and contribute to the basic understanding to the dynamics and confinement of plasma trapped by a dipole magnetic field that may be relevant to space plasma. LDX also incorporates superconducting magnets. While magnetic levitation is now appreciated by many, never before has such a large magnet been levitated by a coil at such a great distance.

As a consequence, LDX has already attracted considerable public attention. Articles discussing the LDX experiment have appeared in the New York Times (Browne, 1999 and Glanz, 1999),

Science Magazine (Riordan, 1999), Lufthansa Magazine (2001), Newton Magazine (Italy, 2001), Popular Mechanics (Wilson, 2002), Wired News (Metz, 2004) and the Technology Review (Vatz, 2005). The NPR program "Here and Now" featured a story on LDX (Gellerman, 1999) and is in the process of creating another story for the program "Living on Earth" (Gellerman, 2005). The Boston Science Museum is presently designing an exhibit describing the LDX.

The research opportunities of the dipole concept has attracted the involvement of several undergraduate and four graduate students at MIT and Columbia and MIT's Department of Nuclear Engineering devoted a part of its innovative fusion engineering course to the dipole concept. LDX has hosted three DOE undergraduate fusion fellows. LDX has also hosted two visiting scientists from Japan and Germany and the proposed budget helps to continue these international collaborations.

Acknowledgement

This proposal represents important contributions, ideas, and suggestions, from a number individuals. We wish to gratefully acknowledge the advice and information provided by Allen Boozer (Columbia), Leslie Bromberg (MIT), Phil Michael (MIT), Joseph Minervini (MIT), Gerald Navratil (Columbia), Miklos Porkolab (MIT), Joel Schultz (MIT) and Brad Smith (MIT), Stewart Zweben (PPPL).

5 Explanation of Budget

The proposed Columbia University and MIT budgets for LDX is adequate for the proposed four-year research plan. Approximately one-third is granted to Columbia University supporting majority of the experimental research staff, one graduate student, and the liquid helium and cryogens. Two-thirds is granted to MIT to support the majority of the engineering and technical staff, operational components and supplies, equipment for diagnostics and plasma control tools, and three graduate students.

A table is provided on the following page summarizing the combined LDX Project staff and budget. The project supports in part the scientific staff (Drs. Garnier, Hansen, Kesner, and Mauel), partial support for Dr. Zhukovsky who directs our engineering and cryogenic operations, two technical associates, and four graduate students. This staffing level is required in order to conduct experimental operations, experimental maintenance, installation of new research tools, and execution of the projects research and educational program.

Other costs include: (i) materials and supplies ($40k/year) for laboratory, vacuum, and electronic components and materials needed to conduct our research program and maintain the LDX facility and for research-related office supplies and telephone charges, (ii) liquid helium ($100k/year) needed to operate the superconducting magnets, (iii) graduate tuition ($74k/year), (iv) domestic travel to attend scientific and technical conferences (estimated nine individual-meetings/year), to allow Dr. Mauel to participate and co-direct activities at MIT, and to visit vendors, and (v) other costs including publication charges and computer and laboratory services needed to support the PSFC. The amounts of these charges correspond to our known expenditure rates.

The final proposed project costs involved the purchase and installation of equipment used for plasma heating, transport physics studies, and diagnostic improvements.

Plasma Heating Equipment Two-thirds of our equipment budget ($326k/3 years) will be used to install additional plasma heating sources. We estimate $101k will be needed for all components and power supplies needed to make operational our existing 18 GHz 15 kW DC Varian klystron and our existing 28 GHz 10 kW DC (100 kW pulsed) Varian gyrotron. These two microwave sources were previously used in the Tara tandem mirror project. The costs include microwave transmission lines, vacuum windows and interface, tube protection and monitoring sensors, and regulated DC high-voltage power supplies. We estimate approximately $250k will be needed for a 100 kW pulse heating source that is capable of plasma heating at high-density. This cost estimate was provided by Dr. A. A. Ivanov (Budker Institute, Russia) for the delivery and commissioning of a 20 ms, hydrogen neutral beam. As described in the proposal, the type of high-density plasma heating source purchased will depend upon the parameters achieved during our density and fueling studies and the outcome of a design study.

Transport Physics Equipment We request $69k/2 years for the fabrication and installation of equipment used to study dipole confinement physics. A fast gas and Li pellet injection system will consist of multiple supersonic gas nozzles with fast-opening piezoelectric (PV-10) valves, a Li pellet injector, and vacuum interface components. Fast gas nozzles will be located both at the outer edge and the high-field regions of the chamber. The Li pellet injector will be constructed to launch pellets either horizontally or vertically. The Li pellet design will follow the designed built by Garnier for the Alcator C-MOD device. Symmetric and asymmetric electrostatic potentials will be excited by biased probes inserted at the edge of the plasma. This system ($10k) requires probe hardware, high-voltage vacuum feedthroughs, and the purchase of three high-voltage DC power supplies (1 kV, 1 A). Asymmetric magnetic fields will be created with a programmable field-error system ($10k) consisting of eight saddle coils mounted directly on the outside of the LDX vacuum chamber (made from standard multi-stranded cable) and eight programmable solid-state

switching power supplies will be purchased (50 V, 100 A). Finally, the control of electrostatic and magnetostatic asymmetries will be explored by applying a pulsed 5-25 kA axial current system ($19k) that requires the fabrication of 10 kJ capacitor bank, vacuum insulators, and a modification to our launcher system.

Diagnostic Equipment We request $92k/2 years for improvements and enhancements to our diagnostic system. This includes $34k to duplicate our single channel 60 GHz microwave interferometer with additional channels, $18k for a neutral particle energy analyzer in order to diagnose ion heating, and $40k for an array of visible spectrometers to image the time-evolution of the radial impurity profile and to measure impurity flow rates with a high-throughput Doppler spectrometer.

Combined LDX Project Staff (FTE's) and Budget ($1,000's)

	FY06	FY07	FY08	FY09
Scientific Staff	2.7	2.7	2.7	2.7
Engineering Staff	0.6	0.6	0.6	0.6
Technical Staff	2.0	2.0	2.0	2.0
Graduate Students	4.0	4.0	4.0	4.0
Total FTE	9.3	9.3	9.3	9.3
MIT Salaries	436	454	472	491
Columbia University Salaries	260	271	282	290
Graduate Tuition	70	73	77	80
Materials and Supplies	38	39	40	41
Liquid Helium	87	96	104	115
Travel (Domestic)	33	33	34	34
Other	34	34	35	36
Plasma Heating Equipment				
Microwave Components and Power	101			
High-Density Heating Source		125	125	
Transport Physics Equipment				
Gas and Pellet Injection	30			
Edge Biasing	10			
Error Field Coils		10		
Axial Current		19		
Diagnostic Equipment				
Interferometry Array	34			
Charge Exchange	18			
Spectroscopy and Imaging		40		
Total Equipment	193	194	125	0
Indirect Costs	390	407	423	440
Total	1,542	1,601	1,591	1,527

6 Management Plan

The LDX project is a joint collaborative project of Columbia University and the Plasma Science and Fusion Center (PSFC) at MIT. The project benefits from strong institutional support from both Columbia University and MIT.

The LDX project is jointly directed by Drs. Michael Mauel and Jay Kesner. Experimental operations are directed by Dr. Darren Garnier. The engineering support is provided by Dr. Alex Zhukovsky, a magnet and cryogenics expert.

The LDX research team has included magnet technology and cryogenics experts as well as plasma scientists making it unique within the U.S. fusion science program. LDX supports two full-time technicians, Rick Lations and Don Strahan, and provides 60% support for a leading magnet research engineer, Drs. Alexander Zhukovsky. During the design and assembly of LDX, Dr. Garnier assisted Dr. Minervini in coordinating the installation of experimental systems. Dr. Garnier is assisted by Dr. Alex Hansen and four graduate students (Ishtak Karim, Eugenio Ortiz, Jennifer Ellsworth, and Alex Boxer). Dipole physics is directed by Dr. Kesner. The MIT theory group under Dr. Peter Catto has also been actively involved in the development of dipole related theory. Columbia University's experience with the mechanically-supported CTX device [38]-[43] and with electron cyclotron resonance heating has guided the LDX design and research plans.

Two international collaborators have so far worked with LDX. These are (1) Prof. Yuichi Ogawa (University of Tokyo) who has interacted on many occasions sharing experiences during the construction of Mini-RT levitated dipole device, and (2) Dr. Olaf Grulke (IPP Greifswald) who spent one year at LDX with support from a Humbolt Fellowship.The present membership of the LDX team is listed in the table on the following page. Research thesis for degrees obtained by MIT students are listed in the Bibliography.

Members of the LDX Research Team

M. Mauel	Columbia	Co-PI
J. Kesner	MIT	Co-PI
Engineering and Superconducting Magnets		
A. Zhukovsky	MIT	Cryogenics
Experimental Operations		
D. Garnier	Columbia	Head
A. Hansen	Columbia	ECRH, Diagnostics
Dipole Physics		
J. Kesner	MIT	Head
Technical Support		
R. Lations	MIT	Cryogenics, Electromechanical
D. Strahan	MIT	Mechanical, Welding
Graduate Students		
I. Karim	MIT	Magnetics, Equilibrium
E. Ortiz	Columbia	Edge Probes, Edge Potential Control
J. Ellsworth	MIT	X-ray Imaging, Pulse-Height
A. Boxer	MIT	Interferometry
Visiting Student		
Emmanuel Mimoun	Ecole Normal Suprieure, Paris	Spectrometer, Visible light
Charles Biddle-Snead (MIT Undergrad)	Columbia U	Control System
Visiting Scientists		
Y. Ogawa	U. Tokyo	Magnets, Dipole Physics

7 Facilities and Other Resources

The LDX experiment is located in the south end of the west cell in MIT PSFC building NW21– adjacent to the Pulse Test Facility (PTF) and within the same building as Alcator C-Mod. The experimental hall occupies one-third of space previously used for the TARA experiment. Because this research space has in place power supplies, power and cooling utilities, cyrogenic systems, and a large overhead crane, MIT's PSFC is an ideal location for LDX.

During the assembly of the LDX device, motivated major investments have been made by PSFC and MIT to further enhance the site and benefit superconducting magnet testing and operation. A helium recovery system has been installed permitting low-cost purchase and re-use of liquid helium from MIT's on-campus liquefier. MIT also provided the installation of new experiment access decking that incorporates supports for x-ray shielding and permit scientists safe and convenient access to the large LDX vacuum vessel.

While the site and infrastructure at the MIT PSFC is particularly well-suited for the LDX experiment, without any doubt, the two most important capabilities of the LDX project are (1) the members of the LDX research team and (2) the three superconducting magnet systems. The appendix, entitled "Facilities and Budget" provide longer descriptions of the magnets and systems that will be used for the proposed experiment.

The LDX Device

In contrast to levitron devices that successfully operated with levitated coils several decades ago [36, 37, 33], a critical design goal of LDX was to maximize the expansion of magnetic flux. LDX requires the levitation of a relatively small coil within a large vacuum chamber. The large distance between the floating coil and the vessel and control magnets represented a design challenge. LDX, however, does not require strong toroidal and vertical fields and this greatly simplifies the stability and control of the LDX floating coil. Our base case magnet configuration, shown in Fig. 2, achieves ring levitation using a single, high temperature superconducting magnet. The floating coil's orientation is stable to tilt and horizontal displacements and, as a result, LDX only requires feedback control to stabilize a slow ($\gamma \sim 4\ \mathrm{s}^{-1}$) instability in floating coil's vertical position. LDX uses a pneumatic "launcher", designed at PPPL, to mechanically lift the floating coil from the bottom of the vacuum vessel (from the so-called "charging station") to the center of the vacuum vessel. At this location, the coil's weight is counterbalanced by the levitation coil located at the top of the vacuum vessel. In effect, the floating coil hangs like a pendulum.

Careful design of the floating coil's cryostat and a method to induce the coil's very large current (> 1 MA) was necessary. The floating coil's cryostat borrows some of the ideas used in the superconducting FM-1 ring built over 30 years ago at PPPL [36, 35]. The FM-1B coil was able to levitated for more than 10 hours a day. The method we've selected to charge the floating coil's large current is induction. As a consequence, there are no high-current electrical contacts that need to be made and broken on the floating coil.

Perhaps, the best way to appreciate the operation of LDX is to view an informative animation located at `http://www.psfc.mit.edu/ldx/ldx_daily_op.html`, and it illustrates a "Day in the Life of LDX." At the beginning of each day, the floating coil is resting within the charging station and precisely centered inside the bore of the large NbTi "charging coil". The floating coil is connected to inlet and outlet cryogenic transfer tubes and a multi-pin temperature-monitoring connector. While the floating coil is resistive (near 20 °K) the charging coil is energized to maximum current. Then, liquid Helium is used to chill the floating coil to approximately 4.5 °K at which time the charging coil current is gradually ramped down. The vacuum tubes and connector to

the floating coil are withdrawn and the coil heat exchanger is evacuated and plugged. With the floating coil now fully charged and disconnected, the pneumatic launcher lifts the coil into position. The levitation coil current is switched on to balance the weight from the launcher. Eight lasers monitor the position of the floating coil, and a real-time digital feedback system controls the current in the levitation and control coils. The "catcher" that cradles the floating coil is now retracted, and plasma experiments begin. At the end of the day, the procedure is reversed, discharging the floating coil and reheating it to approximately 20 °K. Then the charging coil is discharged. A brief description of the superconducting coils appears below:

Superconducting Floating Coil The floating coil (F-coil) is a superconducting magnet comprised of a single 1.5 km length conductor carrying up to 1.5 MA turns in a persistent mode. The design of this conductor, coil and its cryostat was based on many of the advances in superconducting magnet technology made over the past 25 years and now widely used in large numbers of commercial MRI, NMR and other high field magnet systems in reliable, long term operating service worldwide.

The technologies utilized in the F-coil design include:

- High critical current density, low loss, high stability Nb_3Sn conductor,
- Inductive charging arrangement with one very low resistance joint,
- Very low heat loss cryostat design and
- High load, low heat leak laminated crash supports
- Indirect cooling by a flow heat exchanger with re-sealable helium transfer ports.

Optimum combination of these technologies will allow for up to a 2 hour levitation time.

High Temperature Superconducting Levitation Coil. This floating coil is supported by a levitation coil (L-coil) which is located on the top of the vacuum vessel. In addition to providing the magnetic force to levitate the 550 kg floating coil, the L-coil must also be modulated with a feedback signal to provide vertical stability. In the initial LDX machine design, the levitation coil was a water-cooled copper solenoid, and was a substantial continuous load on the available (0.6 MW) cooling water system. With the help of a SBIR with American Superconductor Corporation (ASC), we have designed and fabricated a high temperature superconducting (HTS) levitation coil, which will be the first HTS coil to be used in a US fusion program. The coil winding and cryostat was manufactured at Everson Electric Company, in Bethlehem, PA.

High Temperature Superconducting Levitation Coil This floating coil is supported by a levitation coil (L-coil) which is located on the top of the vacuum vessel. In addition to providing the magnetic force to levitate the 600 kg floating coil, the L-coil must also be modulated with a feedback signal to provide vertical stability. In the initial LDX machine design, the levitation coil was a water-cooled copper solenoid, and was a substantial continuous load on the available (0.6 MW) cooling water system. With the help of a SBIR with American Superconductor Corporation (ASC), we have designed and fabricated a high temperature superconducting (HTS) levitation coil, which will be the first HTS coil to be used in a US fusion program.

Vacuum Vessel. The LDX vacuum vessel, shown in Fig. 2, is a 5 m diameter by 3 m high non-magnetic, 304L stainless steel vessel. It was fabricated using two ASME flanged and dished heads with an interconnecting cylinder and is 1.9 cm (3/4-inch) thick. The vessel is supported below the cylindrical section by six aluminum 6061-T6 legs. Two 1.25 m diameter axial ports, one on the top and one on the bottom, are provided for installing the floating coil and other large internal structures. The vessel also incorporates an array of ten 16.5-inch diameter radial diagnostic ports on the cylindrical section and a set of four 10-inch diameter ports on the top and bottom heads.

A separate 10-inch port is located on the top axial port cover for mounting the launcher catcher. In addition two 24-inch diameter ports provide ports for manned access and large cryopumps. The large size of the vacuum vessel provides excellent access for a variety of plasma heating and diagnostics systems.

Vacuum Systems and Particle Control. The vacuum pumping system consists of a gate valve for isolation, a 1000 l/s turbo pump with a 60 CFM backing pump. In addition, a 300 CFM roughing pump and 1000 CFM Roots blower is available for initial system pumpdown. Two 22-inch cryopumps are used to maintain a base-pressure without plasma to $< 10^{-8}$ Torr. Numerous pressure gauges are included to monitor vacuum throughout the system and a residual gas analyzer is installed to aid in system debugging. Much of the system is controlled by a programmable logic controller (PLC) for remote and automated operation and monitoring. A glow discharge cleaning (single electrode, 7 kW DC) is used routinely for vacuum conditioning.

Plasma Formation, Heating, and Fueling

LDX high-beta plasma is created using multiple-frequency electron cyclotron resonance heating. The dipole magnetic field is known to be stable to high-beta plasmas with energetic particles, and ECRH has proven to be a reliable and low-cost technique to create hot electron, $\beta \sim 1$, plasmas in magnetic mirrors. Furthermore, we have gained important experience from the successful production of hot electrons plasmas in Columbia's CTX experiment [38, 43]. Initially, neutral gas is injected with fast piezo-electric puff valves as was done in CTX. In order to investigate effects of density profiles, an inner, remotely triggered, gas valve and a Li pellet injector will be installed midway through the proposed project period.

We have implemented the resonant microwave heating of electrons as the plasma heating and formation technique best suited for the production of high beta plasmas in LDX. Multiple frequency electron cyclotron resonance heating creates a flexibility that is desirable for adjusting the radial location of the microwave heating and for the enhancement of the production of energetic electrons [74]. LDX generates relativistic electrons, and harmonic absorption appears to be strong. Five microwave sources are available to the LDX experiment. Systems presently operative are a 6.4 GHz Varian klystron (3 kW CW) originally used at Columbia University for plasma processing and a 2.45 GHz klystron (3 kW). A 10.5 GHz klystron (10 kW CW) originally used in the Constance mirror experiment, is being readied for installation this summer. Additional systems that will be implemented during the proposal period include a 28 GHz Varian gyrotron (200 kW, 100 ms and 5 kW CW) originally used for the Tara tandem mirror experiment, an 18 GHZ Varian klystron (20 kW CW) also used for Tara.

Diagnostics and Data Analysis

Common diagnostics will be used to measure global plasma equilibrium (including stored energy and pressure profile), plasma density, hot electron energy, plasma fluctuations and instabilities, neutral particle sources, and edge plasma characteristics. These diagnostics are relatively low-cost and take advantage of the good access provided by the dipole geometry and the LDX vacuum vessel. This approach is appropriate for first-ever investigations where limiting processes and general features of high-beta confinement and stability must be observed. Most of these diagnostics have already been designed, and many have already been built and will be installed during the present grant period.

A list of the LDX diagnostics are:

- Magnetic diagnostics are used for equilibrium reconstruction and magnetic fluctuations. Included are 8 flux loops, 18 Hall probes and 18 pick-up coils.
- X-ray diagnostics are used to measure the energy, intensity, and profile of the energetic electrons. Included are pulse-height counters and an intensified x-ray imaging camera borrowed from the PPPL.
- Adjustable Langmuir probes and probe arrays are used to measure the edge plasma parameters, the electrostatic potential and potential fluctuations. These probes are mounted onto motorized bellows. Gate valves allow various probe types to be used without venting.
- Visible light, with and without D_α filters, and photography is used to view features of the plasma equilibrium, boundary, and gross dynamics.
- Multi-cord microwave interferometry will be used to measure the density and estimate the density profile. The first cord is installed and operates at 60 GHz with a superheterodyne receiver.
- An optical spectroscopy detector array will be installed in order to measure impurity and plasma convection.
- A multi-cord doppler spectrometer will be installed. We plan to make use of the novel, high-throughput line-spectrometer developed by S. Paul [82] that uses interference line filters.
- Neutral particle energy analyzer will be installed midway through the proposed project year to measure T_i in high-density plasma.

These diagnostics are digitized, processed, and archived using MDS-Plus and standard software tools convenient for students and scientists. The critical derived quantities result from magnetic equilibrium reconstruction, pulse-height analysis of the hard x-ray spectrum, and Abel inversion of line-integrated density.

Bibliography

[1] J. Kesner and M. Mauel, "Plasma Confinement in a Levitated Dipole", *Fizika Plazmy* (Plasma Physics Reports), **23** (1997) 801.

[2] D.T. Garnier, J. Kesner, M.E. Mauel, "Magnetohydrodynamic stability in a levitated dipole," Phys. Plasmas **6**, 3431 (1999).

[3] J. H. Schultz, J. Kesner, J. Minervini, A. Radovinsky, S. Pourrahimi, B. Smith, P. Thomas, P. Wang, A. Zhukovsky, R. Myatt, S. Kochan, M. Mauel, and D. Garnier, "The Levitated Dipole Experiment (LDX) Magnet System," *IEEE Trans. Appl. Supercond.*, **9** (1999) 378.

[4] A. Zhukovsky, M. Morgan, D. Garnier, A. Radovinsky, B. Smith, J. Schultz, L. Myatt, S. Pourrahimi, J. Minervini, "Design and Fabrication of the Cyrotstat for the Floating Coil of the Levitated Dipole Experiment (LDX)", *IEEE Trans. Appl. Supercond.*, **10** (2000) 1522.

[5] B.A. Smith, J.H. Schultz, A. Zhukovsky, A. Radovinsky, C. Gung, P.C. Michael, J.V. Minervini, J. Kesner, D. Garnier, M. Mauel, G. Naumovich, and R. Kocher, "Design, Fabrication and Test of the React and Wind, Nb3Sn, LDX Floating Coil", *IEEE trans. Appl. Supercond*, **11** (2001) 2010.

[6] A. Zhukovsky, J. Schultz, B. Smith, A. Radovinsky, D. Garnier, O. Filatov, V. Beljakov, S. Egorov, V. Kuchinsky, A Malkov, E. Bondarchouk, V. Korsunsky, V. Sytnikov, "Charging Magnet for the Floating Coil of LDX", *IEEE Trans. Appl. Supercond.*, **11** (2001) 1873.

[7] A. Zhukovsky, D. Garnier, C. Gung, J. Kesner, M. Mauel, P. Michael, J. Minervini, M. Morgan, T. Pedersen, A. Radovinsky, J. Schultz, B. Smith, *IEEE Trans. Appl. Supercond.*, **12** (2002) 666.

[8] D. D. Ryutov, J. Kesner, and M. E. Mauel, *Phys. Plasmas*, **11** (2004) 2318.

[9] J. Ellsworth, *X-Ray Diagnostics for the Levitated Dipole Experiment*, MS Dissertation (MIT, 2004).

[10] A. Roach, *Floating Coil Position Detection System for the Levitated Dipole Experiment*, B.S. Dissertation, (MIT, 2005).

[11] S. Mahar, *Multiple Frequency ECH for the Levitated Dipole Experiment*, M.S. Dissertation, (MIT, 2005).

Dipole Fusion Concept References:

[12] A. Hasegawa, Comm Pl Phys & Cont Fus, **1**, (1987) 147.

[13] A. Hasegawa, L. Chen and M. Mauel, Nuclear Fus. **30**, (1990) 2405.

[14] A. Hasegawa, L. Chen, M. Mauel, H. Warren, S. Murakami, Fusion Technology **22** (1992) 27.

[15] E. Teller, A. Glass, T.K. Fowler et al., Fusion Technology **22**, (1992) 82.

[16] V. Pastukhov and A. Yu. Sokolov, Nuc. Fusion **32** (1992) 1725.

[17] A. Yu. Sokolov, Plasma Phys. Rep. 19 (1993) 1454.

[18] S. I. Krasheninnikov, P. Catto, R. D. Hazeltine, *Phys. Rev. Lett.*, **82** (1999) 2689.

[19] A.N. Simakov, P.J. Catto, S.I. Krasheninnikov, J.J. Ramos, Phys. Plasmas **7**, 2526 (2000).

[20] J. Kesner, Phys. Plasmas **7**, 3837 (2000).

[21] J. Kesner, D.T. Garnier, Phys. Plasmas **7**, 2733 (2000).

[22] V.P. Pastukhov, Plasma Physics Reports **26**, 529 (2000).

[23] A. Simakov, P. Catto, R.J. Hastie, Phys. Plasmas **8**, 4414 (2001).

[24] V.P. Pastukhov and N.V. Chudin, Plasma Physics Reports **27**, 907 (2001).

[25] A. Simakov, P. Catto, R.J. Hastie, J.J. Ramos, Phys Plasmas **9**, 4985 (2002).

[26] J. Kesner, R.J. Hastie, Phys. Plasmas **9**, 4414 (2002).

[27] A. Simakov, R.J. Hastie, P. Catto, Phys. Plasmas **9**, 201 (2002).

[28] A.B. Mikhailovsky and A.A. Skovoroda, Plasma Phys. Cont. Fusion, **44**, (2002) 2033.

[29] J. Tonge, C. Huang, J.N. Leboeuf and J.M. Dawson, *Phys. Plasmas*, **10** (2003) 3475.

[30] V.P. Pastukhov and N.V. Chudin, 19th IAEA Fusion Energy Conf, Paper IAEA-TH/2-5, *Fusion Energy 2002*, Lyon, France (International Atomic Energy Agency, Vienna 2003).

[31] J. Kesner, Phys. Plasmas **10**, 908 (2003).

[32] J. Kesner, D.T. Garnier, A. Hansen, M. Mauel, L. Bromberg, Nucl. Fusion **44** (2004) 193.

Other Dipole Confinement Related Experiments:

[33] O .A. Anderson, *et al.*, in *Plasma Physics and Controlled Nuclear Fusion* (IAEA, Vienna, 1972) Vol. 1, 103.

[34] D.E. Lencioni, *et al.*, Phys. Fluids **11** (1968) p. 1115.

[35] See reports describing design and operation of FM-1 in *Proceedings, Fourth Symposium on Engineering Problems of Fusion Research*, (NRL, Washington, D.C., April 20-23, 1971) I.E.E.E., New York, pp. 83-101, 273-290, and 351-380.

[36] R. Freeman, *et al.*, "Confinement of plasmas in the spherator", in *Plasma Physics and Controlled Nuclear Fusion Research* (IAEA, Vienna, 1972) Vol. 1, 27.

[37] M. Okabayashi, *et al.*, Phys. Fluids **16** (1973) 1337.

[38] H. P. Warren and M. E. Mauel, Phys. Rev. Lett. **74** (1995) 1351.

[39] H. P. Warren and M. E. Mauel, Phys. Plasmas **2**, 4185 (1995).

[40] H. P. Warren, M. E. Mauel, D. Brennan, and S. Taromina, Phys. of Plasmas **3** (1996) 2143.

[41] M.E. Mauel, Journal de Physique, IV **7**, (1997) 307.

[42] P. J. Catto and S. Krasheninnikov, *Phys. Plasmas*, **7**, 1452 (2000).

[43] B. Levitt, D. Mastovsky and M. Mauel, Phys. Plasmas **9**, (2002).

[44] D. Maslovsky, B. Levitt, M. Mauel, *Phys. Rev. Lett.*, **90** (2003) 185001.

[45] Yanagi, N. ,Mito, T.; Morikawa, J.; Ogawa, Y.; Ohkuni, K.; Hori, D.; Yamakoshi, S.; Iwakuma, M.; Uede, T.; Itoh, I.; Fukagawa, M.; Fukui, S., "Experiments of the HTS floating coil system in the mini-RT project", IEEE Transactions on Applied Superconductivity, v 14, n 2, June 2004, p 1539-42.

[46] B. Levitt, M. Mauel, D. Maslovsky, *Phys. Rev. Lett.*, **94** (2005) 175002.

[47] B. Levitt, M. Mauel, D. Maslovsky, J. Waksman, *Phys. Plasmas*, **12** (2005) 055703.

[48] N. Krasheninnikova, P. Catto,"Effect of Hot Electrons on the Stability of a Closed Field Line Plasma", to be published in Phys. Plasmas (2005)

Plasma Physics References:

[49] M.N. Rosenbluth and C.L. Longmire, Ann. Phys. **1**, 120 (1957).

[50] I.B. Bernstein, E. Frieman, M. Kruskal, R. Kulsrud, Proc. R. Soc. Lond. A **244** 17 (1958).

[51] T. Gold, *J. Geophys. Res.*, **64** (1959) 123.

[52] I. A. Daglis, R. M. Thorne, W. Baumjohann, S. Orsini, Rev. Geophys., **37**, 407 (1999).

[53] B. Lehnert, Nature **181** (1958) 331.

[54] T. Hellsten, Physica Scripta, **9** (1976) 313.

[55] J. Van Allen, *et al.*, *Jet Propulsion* **28** (1958) 588.

[56] M. Schulz and L. Lanzerotti, *Particle Diffusion in the Radiation Belts*, (Springer, 1974).

[57] C. T. Russel, "The Dynamics of Planetary Magnetospheres," Planetary and Space Science, **49** (2001) 1005.

[58] S. Elkington, *et al.*, *J. Atmosph. and Solar-Terrestrial Physics*, **66** (2004) 1371.

[59] A.M. Rey and A.B. Hassam, Phys. Plasmas **8**, 5151 (2001).

[60] J. Feron et al, Phys. Plasmas **26** (1983) 2227.

[61] R.H. Kraichnan, Phys Fluids **10**, (1967), 1410.

[62] A. Hassam and R. Kulsrud, Phys Plasmas **22**, (1979) 2097.

[63] J. M. Dawson, H. Okuda and R. Carlile, Phys. Rev. Lett. **27** (1971) 491

[64] J. Drake, J. Greenwood, G. Navratil, R.S. Post, Phys Fluids**201** (11977) 148.

[65] T. Jernigan, J. Rudmin and D. Meade, PRL **26** (1971) 1298.

[66] R. A. Dandl *et al.*, Nucl. Fusion **4** (1964) 344.

[67] N. Krall, Phys. Fluids **9** (1966) 820.

[68] H.L. Berk, Phys. Fluids **19** (1976) 1275.

[69] D.B. Nelson, Phys. Plasmas **23**, (1980) 1850.

[70] J. Van Dam and Y.C. Lee, *Proc. Workshop on EBT Ring Physics*, ORNL Report 791228 (1979).

[71] D. Batchelor, Nuc. Fusion **21** (1981) 1615.

[72] S. Hiroe, J.B. Wilgen, T.W. Baity, L.A. Berry, R.J. Colchin, et al., Phys. Fluids **27**, 1019 (1984).

[73] M. E. Mauel, *Phys. Fluids*, **27** (1984) 2899.

[74] B. Quon et al., Phys. Plasmas, **28**, (1985) 1503.

[75] M.J. Gerver and B.G. Lane, Phys. Plasmas **29**, (1986) 2214.

[76] X. Chen, B. G. Lane, D. L. Smatlak, R. S. Post, and S. A. Hokin, *Phys. Fluids B*, **1** (1989) 615.

[77] R. C. Garner, M. E. Mauel, S. A. Hokin, *et al.*, Physics of Fluids B **2** (1990) 242.

[78] W.M. Nevins, Journal of Fusion Energy **17**, 25 (1998).

[79] R.A. Krakowski, R.L. Miller, J.G. Delene, "Directions for improved fusion reactors", Fusion Reactor Design and Technology 1986, Proceedings of the Fourth Technical Committee Meeting and Workshop, STI-PUB-754. (1987) vol.1, p 265-83. Detailed parameters from http://aries.ucsd.edu/miller/AT31002/output.html.

[80] F. Najmabadi, S. C. Jardin, M. Tillack , L. M. Waganer and the AIRIES Team, "ARIES-AT: An Advanced Tokamak, Advanced Technology Fusion Power Plant", 19th IAEA Fusion Energy Conf, Paper IAEA-CN-77-FTP2/15, Lyon, France (2002), submitted to Fusion Eng. and Design (2003).

[81] G. F. Abdrashitov, *et al.,* Rev. Sci. Instrum. **72** (2001) 594.

[82] S. F. Paul, C. Cates, M. Mauel, D. Maurer, G. Navratil, and M. Shilov, *Rev. Sci. Instruments* **75** (2004) 4077.

[83] J. Connor and R.J. Hastie, Phys. Fluids **19**, 1727 (1976).

[84] A. Simakov, R.J. Hastie, P. Catto, Phys Plasmas **7**, 3909 (2000).